Reducing Socket Discomfort and Torsional Stresses for Individuals With Lower-Limb Amputation Using a Novel Prosthesis

Connor William Mulcahy

A thesis

submitted in partial fulfillment of the

requirements for the degree of

Master of Science in Mechanical Engineering

University of Washington

2021

Committee:

Glenn Klute

Katherine Steele

Sawyer Fuller

Program Authorized to Offer Degree:

Mechanical Engineering

University of Washington

Abstract

Reducing Socket Discomfort and Torsional Stresses for
Individuals With Lower-Limb Amputation Using a Novel Prosthesis

Connor William Mulcahy

Chair of the Supervisory Committee:
Glenn Klute
Mechanical Engineering

Individuals with lower-limb amputation often suffer pain and discomfort at the socket-residual limb interface after using their prosthesis. A portion of this pain and discomfort can be isolated to the transverse plane. It has been shown that the inherent geometry of the bones in the ankle joint produce motion in the transverse plane; however, prosthetic limbs generally only function in the sagittal plane. Torsion adapters are a clinical product used to passively allow rotation in the transverse plane at the pylon level of a prosthesis. These adapters have been shown to relieve skin problems, but they introduce a perceived decrease in stability. Olson made a first iteration Torsionally Active Prosthesis (TAP) in a pilot study which showed that a powered prosthesis operating in the transverse plane can reduce transverse socket torque. The study presented in this thesis continued Olson's preliminary work by iterating on the TAP's design and testing more human subjects. By coupling sagittal plane rotation with transverse plane rotation, this study hypothesizes that there exists a coupling ratio (CR) that minimizes peak transverse-plane socket torque and maximizes user satisfaction. Participants (n=3) tested the TAP under a range of CRs

for three different walking regimes: straight walking, prosthesis inside circle walking, and prosthesis outside circle walking. Initial results suggest a small CR will minimize socket torque within each walking regime. For straight walking, a small or zero CR may minimize socket torque. For circle walking, a small, nonzero CR may also minimize socket torque independent of whether the prosthesis is on the inside or outside limb. Initial results for comfort level showed that changing CRs did not present any trends. Further human subject tests with the TAP are warranted because increasing the comfort level and residual limb health of users is of significant clinical interest.

Table of Contents

List of Figures

List of Tables

List of Equations

List of Abbreviations

TAP ..... Torsionally Active Prosthesis

CR ..... Coupling Ratio

CLiMB ..... Center for Limb loss and MoBility

GRF ..... Ground Reaction Force

HS ..... Heel Strike

TO ..... Toe Off

ST ..... Straight

PI ..... Prosthesis Inside

PO ..... Prosthesis Outside

UD..... Unified Deformable

SCS ..... Socket Comfort Score

Acknowledgements

I would like to thank Glenn Klute for his guidance and for the opportunity to work on this meaningful and fascinating research. I would also like to thank Krista Cyr for her invaluable support in multiple aspects of this project from human participant motion capture experience and experimental design to data processing experience and interpretation. Many thanks to G. Eli Kaufman for his work as a prosthetist in making sure each participant had a comfortable and proper fit when using the Torsionally Active Prosthesis. Thanks also to Elise Campbell and Andrew Ton for coordinating all human participant recruitment and scheduling; without their help there would have been no participants in the study to discuss. None of this would have been possible without everyone's help: thank you all very much.

This research was supported by Dept. of Veterans Affairs, Rehabilitation Research and Development Service, grants RX002974 and RX002456.

Chapter 1:
Introduction

1.1 Background

Human motion can be largely simplified in a manner solely focused on the sagittal plane; this is apparent due to the body of biomechanical research dealing with this plane. True human motion, however, lies in all three planes of movement: sagittal, transverse, and coronal [1], [2]. During gait, humans do have considerable motion in the off-sagittal planes, but the difficulty in studying the frontal and transverse components lies in using modern motion capture techniques, such as passive markers, to record these movements [3], [4]. Researchers need to be able to independently track the relative motion of two bones on the same kinematic chain. They use bony landmarks on the body as references for skeletal motion; this often provides sufficient information for the sagittal plane. The issues with the foot-ankle complex are that the bones are small and that they are often obscured by footwear. This results in no good bony landmarks to track the small bones that make up the major joints of the foot-ankle complex. These major joints do not have good bony landmarks that properly represent their axes of movement. The axes of rotation for the ankle joint do not follow a simple orthogonal coordinate system but instead are angled and skewed off of orthogonal axes due to the inherent geometry of the bones of the ankle [2], [5]. For example, the bone geometry of the talus in the mortise joint causes the foot to adduct at full plantarflexion and abduct at full dorsiflexion. It is with this gap in knowledge in mind that this study proposes to move forward with its research into coupling the sagittal plane with the transverse plane in a novel prosthetic foot.

Individuals with lower-limb amputation are missing key sections of their kinematic chain, which is especially apparent during motion. When focusing on the interface between the socket and the residual limb in individuals with lower extremity amputation during gait, users and

researchers are made aware of the induced discomfort and pain from torsional stresses from this lack of a complete kinematic chain and the rigidity of the prosthesis [6]–[8]. These problems are often derived from transmitted loads that occur during ambulation and may be exacerbated with turning gait [8]. As shown by Orendurff et al. [9], [10], turning is likely more difficult for these individuals with lower-limb amputation because of their inability to modulate transverse plane joint torque, which is one of the turning mechanisms for able-bodied individuals. Torsion adapters, which change the torsional stiffness at the pylon-socket interface, allow for motion in the transverse plane [11]. Studies have shown that using these adapters results in decreased pain and increased comfort [8]. Despite the benefits, a downside to torsion adapters is that they are passive devices whose properties cannot be varied to suit the activity. Segal et al.'s [12] stability analysis of torsion and rigid adapters suggested that individuals with lower-limb amputation are the most unstable using either style of adapter when walking with their prosthetic limb on the inside of a turn when compared to walking with the prosthesis on the outside of a turn or in a straight line. This stability issue is overcome by the user by using inefficient, compensatory techniques during gait. The Torsionally Active Prosthesis (TAP) also functions by rotating in the transverse plane, but since it is an active device, it addresses some of these shortcomings.

The first iteration of the TAP was developed by Olson in 2016 [13], [14]. The motivation of the design came from Lundberg's studies on the arthrokinematics of the ankle joint[4], [15], [16]. These studies showed that there existed significant movement in the transverse plane at the ankle joint. Olson showed that by coupling the sagittal and transverse planes in a powered prosthesis that socket torque could be successfully decreased. This study was only a pilot study (n=3) and did not have a significant sample size to generalize any conclusion. The study presented in this thesis iterated on this work with a second generation TAP that improved the

following aspects: device user interface, electronics, software, and the prosthetic ankle angle sensor.

1.2 Objective

This study focuses on the relationship between the transverse plane and sagittal plane during motion. This relationship is defined in Equation 1.1 below as the coupling ratio (CR). The TAP rotates in the transverse plane by tracking the current position of the user in the sagittal plane. The objective of this study was to decrease the pain and discomfort individuals with lower-limb amputation can experience under undesired torsional loads within the socket. This was accomplished by finding a CR within a hypothesized range that maximizes user comfort and minimizes peak transverse plane socket torque for the study population.

The TAP has multiple software settings that are used to discretely test for a CR that is most comfortable to each user. The CR is defined in Equation 1.1 as

$$\mathrm{CR} = \theta_{TP} : \theta_{SP}$$

Equation 1.1 Coupling Ratio relationship.

where θ_{TP} is transverse plane angle in degrees and θ_{SP} is sagittal plane angle in degrees. A CR of 1:2, for example, would mean that the TAP would rotate 1° in the transverse plane for every 2° of movement in the sagittal plane. In practice, the CR will be replicating the body's internal and external rotation at the ankle. It was hypothesized that a user's preferred CR exists between a CR of 0 and 1:2 that maximizes comfort and minimizes the peak transverse plane moment. To test this hypothesis, the following discrete CRs were tested: 0, 1:6, 1:4, 1:3, and 1:2.

1.3 Thesis Overview

This thesis will present the design, development, human subject testing, and testing results of a novel, torsionally active prosthesis. The system design describes how the mechanical, electrical, and software aspects were developed and interface with each other. The motor controller was developed using hardware-in-the-loop tuning using a fully assembled TAP. Individuals with lower-limb amputation were able to use the fully operational TAP while walking under a series of randomized CRs. The walking types tested were 1-m radius circle walking in both directions and straight walking. The motion capture and TAP-based results from these tests were statistically analyzed using repeated measures ANOVAs.

Chapter 2:
System Design

The TAP operates by using a 60-watt brushed DC motor in series with a 100:1 Harmonic Drive transmission to rotate a low-profile prosthetic foot in the transverse plane at the ankle level (Figure 2.1). As shown in Figures 2.2 and 2.3, strain gauges are installed to the prosthetic foot to sense bending during gait and translate it as user input. Prosthetic foot bending is analogous to an able-bodied foot's sagittal plane plantar- and dorsiflexion. In software, this bending is mapped to a corresponding sagittal plane ankle rotation angle using experimentally-derived equations. This angle is then scaled via a predefined CR to a corresponding transverse plane ankle rotation angle. A PID controller uses this transverse plane angle as a setpoint to control the motor at a loop rate of 1 kHz.

2.1 Overview

The mechanical strength of this device comes from the 60 watt brushed DC motor (RE30, Maxon Precision Motors, San Mateo, CA) that is powered by a 11.1 V 3-cell LiPo battery connected to a motor driver (18v25 CS, Pololu Robotics and Electronics, Las Vegas, NV) (Figures 2.1 and 2.4). The motor torque is amplified by the 100:1 Harmonic Drive (CSF14-2XH-F, Harmonic Drive, Hauppauge, NY). A magnetic encoder (Encoder MR, Type L, Maxon Precision Motors, San Mateo, CA) with 1024 counts per turn monitors the position of the motor. The computational power of this device is in the Teensy 3.6 (PJRC, Sherwood, OR) microcontroller, which features a 32-bit 180-MHz ARM Cortex-M4 processor with floating point unit (Figure 2.5). The controller operates at a 1-kHz loop rate with all the calculations performed using floating point math, leading to a more precise level of control than that offered by integer math. Controller feedback is the motor position given by the encoder. Data is logged

on a microSD card at a sampling rate of 100 Hz. There are four strain gauges in total installed on the prosthetic foot at the following four locations: (1) anterolateral, (2) anteromedial, (3) posteromedial, and (4) posterolateral. These strain gauges are each amplified with load cell amplifiers (SparkFun Electronics, Niwot, CO). As shown in Figure 2.2, the staff testing with the TAP can control the device's power using two rocker switches to regulate power to the custom circuitry and the motor. Once the device is turned on, two rotary switches can control the current CR and multiple testing states.

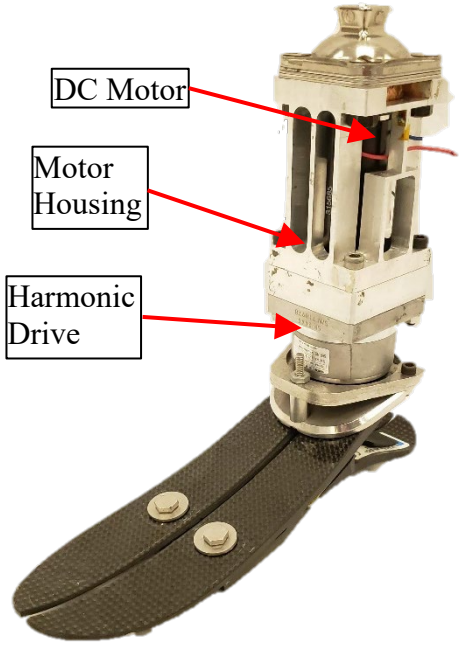

Figure 2.1 The internal hardware without electronics.

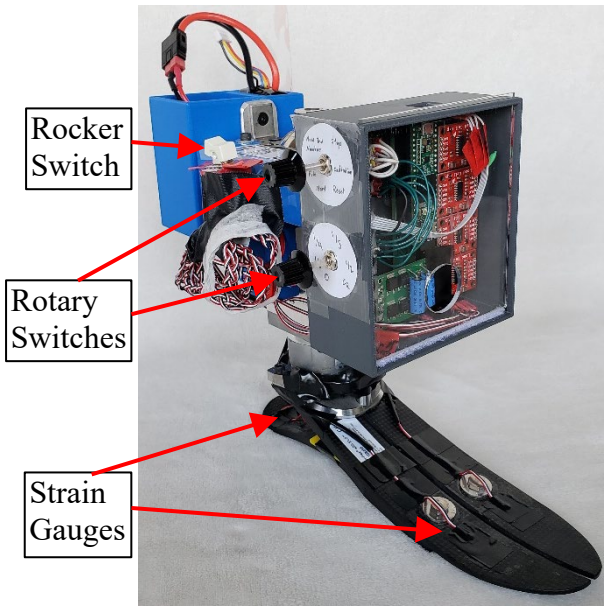

Figure 2.2 User input circuitry front.

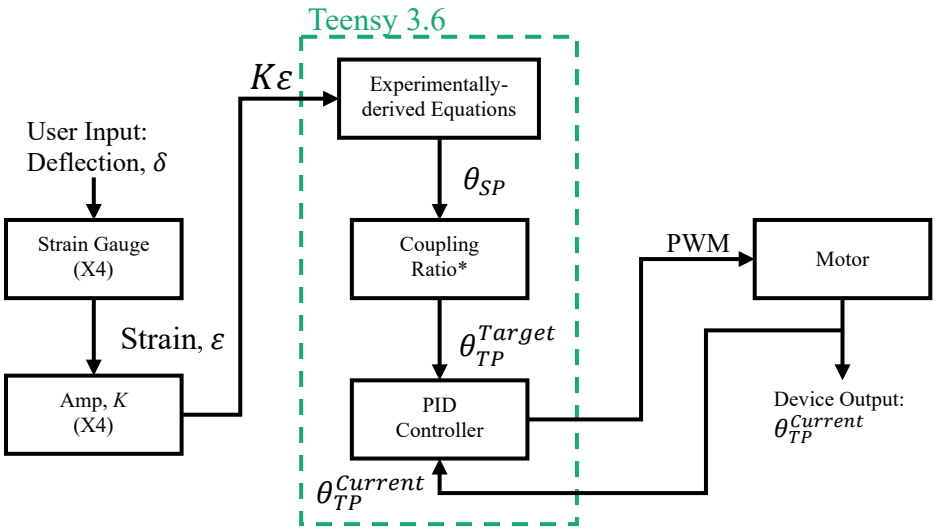

Figure 2.3 System architecture starting from user input and ending with device output. *Coupling Ratio: $CR = \theta_{TP} : \theta_{SP}$.

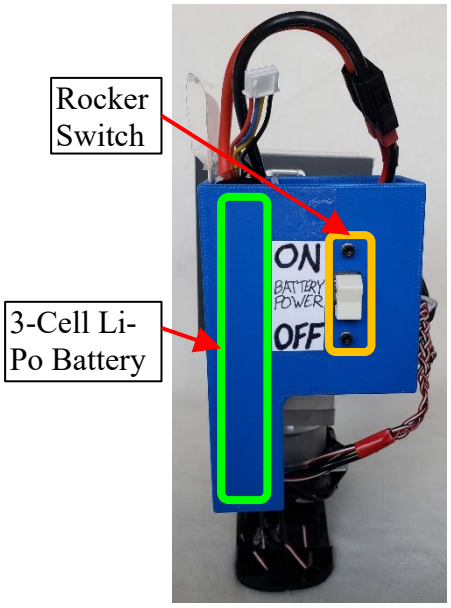

Figure 2.4 User input circuitry back.

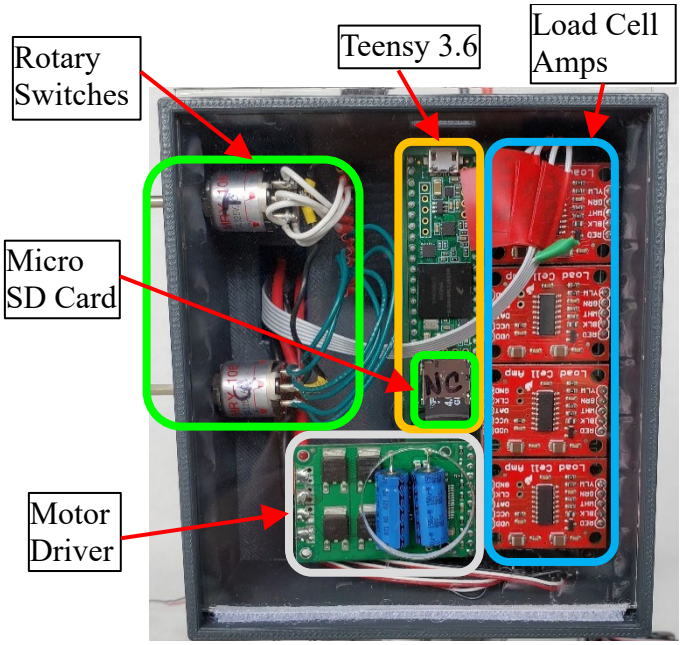

Figure 2.5 The internal circuitry is protected by an acrylic cover that slides up for access to the SD card.

2.2 Mechanical Design

One of the largest considerations in mechanical design of a transtibial prosthesis is build height. This is because the length of residual limb a person could have can vary between individuals. By designing the device to minimize build height, this allows for the largest number of possible users. Originally designed and built by Olson [14], the custom adapter and aluminum motor housing allow for a compact build height. The custom adapter replaces the male pyramid adapter of the prosthetic foot. This allows for the motor and transmission to be as close to the foot as possible without having to work around the male pyramid adapter, resulting in a more compact design and saving build height. The motor housing is load-bearing and allows for the motor to be placed directly inside of the housing. A pyramid adapter can then be placed on top of the device allowing it to interface with common prosthetic sockets. The housing also provides surface area for the necessary electronics housings to be built out laterally.

2.3 Electrical Design

The circuitry of the TAP combines both custom and purchased parts. The main interface that allows the electrical components to interact with each other is a custom PCB, which was designed in EAGLE (Autodesk Inc., San Rafael, CA) (Figure 2.6). The schematic for the PCB is shown in Figure 2.7. This PCB utilizes a custom conditioning circuit implemented using surface mount technology (SMT) components on the bottom of the board to condition any signal sent or received by the daughterboards on the top of the board. The top of the board houses the circuitry for receiving any motor encoder signals, strain gage signals, and rotary switch signals. Each strain gauge is part of a quarter-bridge Wheatstone circuit where the other three resistors of equal resistance are SMT components. The Teensy 3.6 microcontroller operates on a 3.3-V logic level whereas the motor driver operates on a 5-V logic level. Any direct interactions between these

two boards needed to be logic level shifted by a MOSFET circuit. An important signal from the motor driver that could not just be logic shifted was the current sensing signal that outputs an analog 5-V signal centered at 2.5 V at a rate of 66 mV/A. This signal was conditioned for the Teensy using an operational amplifier buffer followed by a voltage divider to scale the signal down to a 2.8-V signal centered at 1.4 V at a rate of 36.9 mV/A. The 11.1-V 3-cell LiPo battery directly powers the motor board and the motor, while all other daughterboards are powered with battery power that has been voltage regulated down to a safe 5 V. The device has a two-phase startup process using two rocker switches to control power. One switch is positioned between the battery and the motor board to regulate power to the control circuitry. The second switch is positioned between the motor board and the motor to regulate power to the motor. This second switch is necessary because of the startup time required by the Teensy's internal control circuitry to set pin definitions; were power not cut off during this time, the motor would receive a maximum control signal and rotate uncontrolled in a direction. This would create a situation where the starting zero position would always be moved on device startup; by splitting the power-up sequence into two phases, system power-up behaves much more consistently.

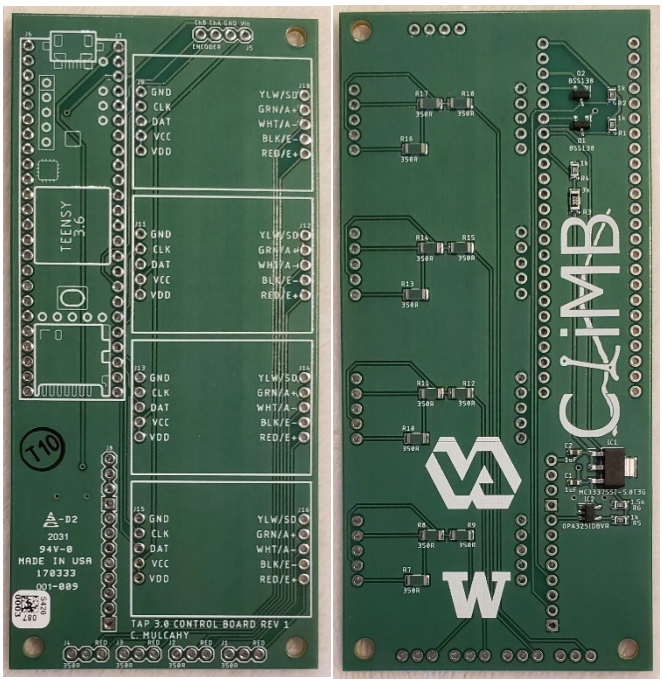

Figure 2.6 TAP 3.0 Control Board Rev 1 top (left) and bottom (right) before any header pins were attached.

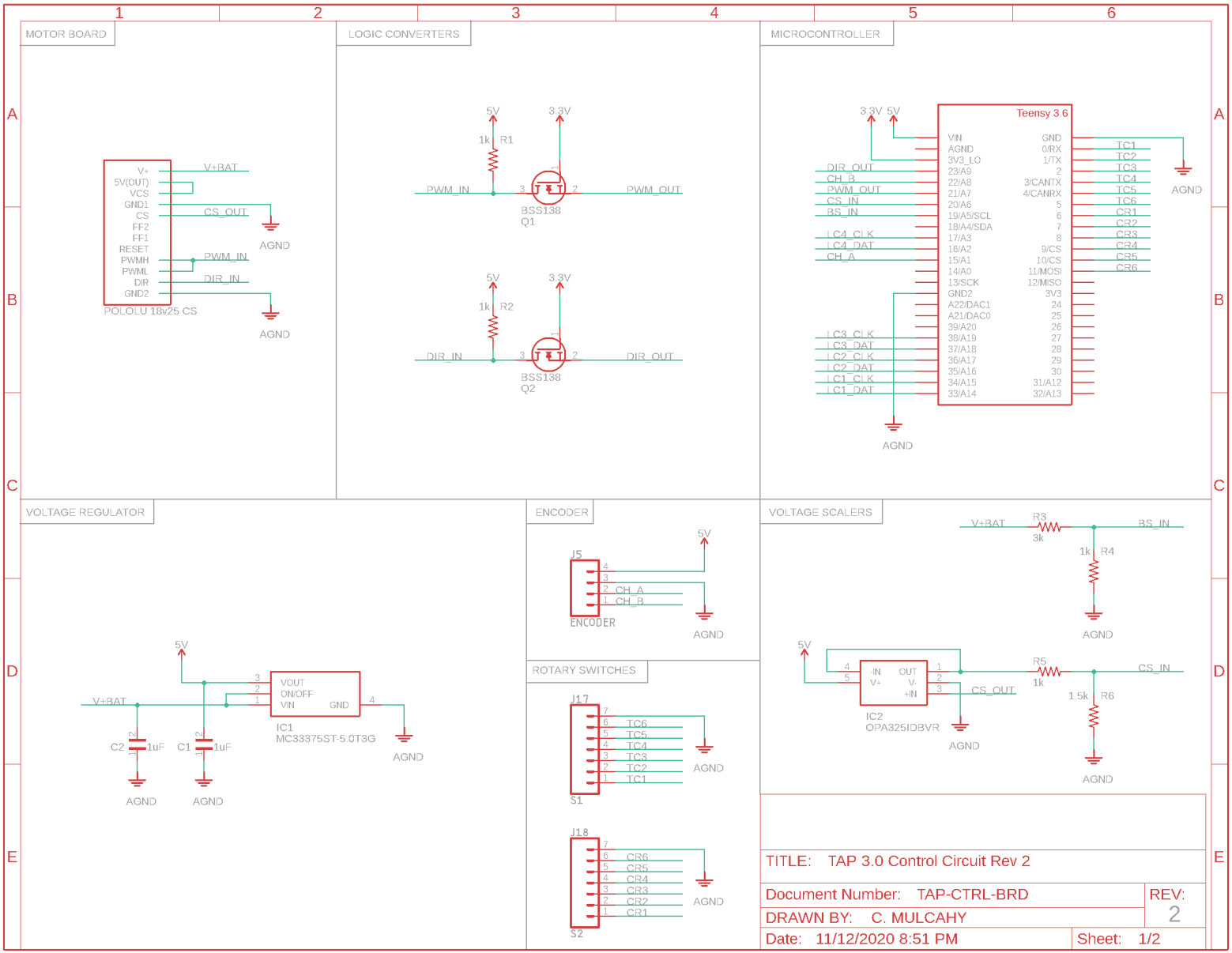
MOTOR BOARD
V+
5V(OUT)
VCS
GND1
CS
FF2
FF1
RESET
PWMH
PWML
DIR
GND2
V+BAT
CS_OUT
PWM_IN
DIR_IN
AGND
AGND
POLOLU 18v25 CS
LOGIC CONVERTERS
5V
3.3V
1k R1
PWM_IN
PWM_OUT
BSS138
Q1
1k R2
DIR_IN
DIR_OUT
BSS138
Q2
MICROCONTROLLER
Teensy 3.6
3.3V 5V
VIN
AGND
3V3_LO
23/A9
22/A8
21/A7
20/A6
19/A5/SCL
18/A4/SDA
17/A3
16/A2
15/A1
14/A0
13/SCK
GND2
A22/DAC1
A21/DAC0
39/A20
38/A19
37/A18
36/A17
35/A16
34/A15
33/A14
GND
0/RX
1/TX
2
3/CANTX
4/CANRX
5
6
7
8
9/CS
10/CS
11/MOSI
12/MISO
3V3
24
25
26
27
28
29
30
31/A12
32/A13
DIR_OUT
CH_B
PWM_OUT
CS_IN
BS_IN
I_C4_CLK
I_C4_DAT
CH_A
I_C3_CLK
I_C3_DAT
I_C2_CLK
I_C2_DAT
I_C1_CLK
I_C1_DAT
TC1
TC2
TC3
TC4
TC5
TC6
CR1
CR2
CR3
CR4
CR5
CR6
AGND
AGND
VOLTAGE REGULATOR
5V
V+BAT
VOUT
ON/OFF
VIN
GND
IC1
MC33375ST-5.0T3G
C2 1uF
C1 1uF
AGND
AGND
AGND
ENCODER
5V
J5
CH_A
CH_B
ENCODER
AGND
ROTARY SWITCHES
J17
TC6
TC5
TC4
TC3
TC2
TC1
S1
AGND
J18
CR6
CR5
CR4
CR3
CR2
CR1
S2
AGND
VOLTAGE SCALERS
V+BAT
R3
3k
BS_IN
1k R4
AGND
5V
IN+
V+
OUT
V-
+IN
IC2
OPA325IDBVR
CS_OUT
R5
1k
CS_IN
1.5k R6
AGND
AGND
TITLE: TAP 3.0 Control Circuit Rev 2
Document Number: TAP-CTRL-BRD
REV: 2
DRAWN BY: C. MULCAHY
Date: 11/12/2020 8:51 PM
Sheet: 1/2

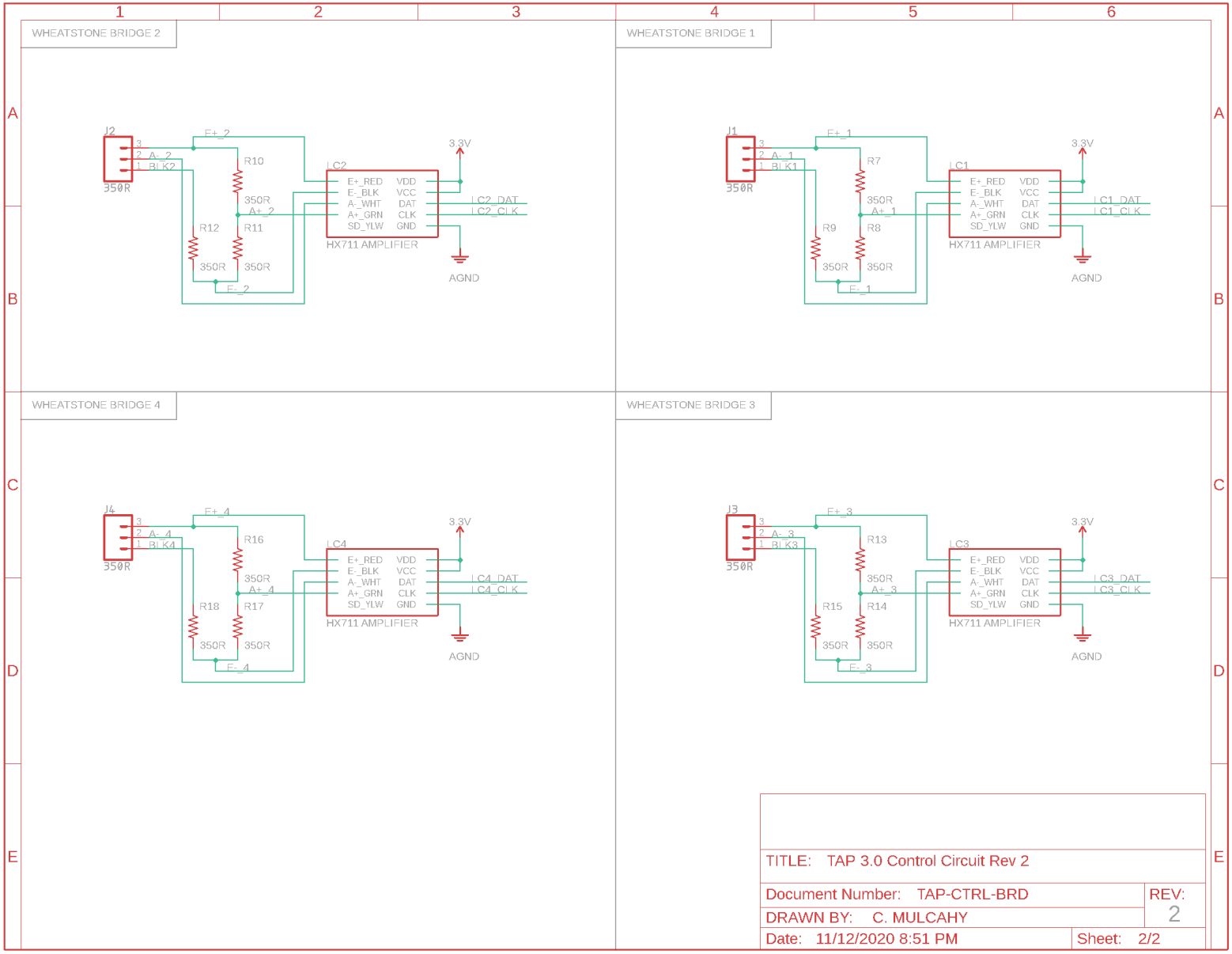

Figure 2.7 Custom PCB schematic. Top is sheet 1 and bottom is sheet 2.

2.4 Software Design

The code uploaded to the Teensy 3.6 microcontroller was written using a software addon for the Arduino API called "Teensyduino," which allows a user to run Arduino-based sketches on Teensy products. The main feature of the microcontroller that this custom code is based around is the *IntervalTimer* class, which uses interrupts to call a function at a precise timing interval. The TAP's main interrupt service routine (ISR) used to control the device is called *controlISR()* and functions at all times after startup. Using an *IntervalTimer* object to call this ISR guarantees that the PID control loop is run every 1 ms or at a rate of 1 kHz. During device calibration, setup, and in between trials, the ISR keeps the motor steady at a 0° position. During testing and data collection, the ISR uses values from the strain gauges with the preset CR to control the motor's position. Another big benefit of using the *IntervalTimer* class to call *controlISR()* every millisecond is that the programmer can create, increment, and use a custom millisecond time variable to avoid any possible quirks that the built-in, Arduino-based *millis()* function might have such as not always increasing at a constant rate.

The TAP can adjust the controller response based on the user's given body weight. The lower rotary switch can be turned to calibration to initiate the process. During calibration, the user is instructed to stand still because the strain gauge values are being cumulatively averaged together to derive an offset value. In software, this process is set to take this cumulative average for an indefinite amount of time, so anywhere between 30 s to 60 s is enough time to reach a steady state offset value. This offset value is analogous to a DC offset in an electrical signal. The offset takes into account both the user's body weight and that the strain gauges are installed on a curved surface giving them an inherent prestrain. This value is then used to adjust the sequentially read strain gauge values used in *controlISR()*.

Chapter 3:
TAP Controller Tuning

The TAP's motor controller was developed in stages with increasing levels of hardware-in-the-loop complexity. Initially a benchtop setup was used to develop the controller. This setup involved fixing the body of the TAP without a prosthetic foot to a benchtop surface and rotating a weighted bar. The weighted bar was designed to a specific moment of inertia value to simulate forced rotation of the shank and thigh. Strain gauges were installed onto the prosthetic foot and used to map strain values to sagittal plane angles. Combining the benchtop controller with the sagittal plane mapping, an able-bodied person was able to use custom walking boots with pyramid adapters to walk on the TAP overground. Overground walking was tested each CR under three walking conditions: straight walking, prosthesis inside circle walking, and prosthesis outside circle walking. TAP transverse angles and motor current analysis showed the importance of fluctuating body weight during stance for controller tuning. Using the same setup as overground, the custom boots were then used over a treadmill to tune the controller under body weight.

3.1 Benchtop Tuning

The PID controller for the TAP's motor started out as a simple Proportional controller and grew in complexity as needed over time. The Teensy 3.6 was chosen for its desirable 32-bit, 180-MHz processor; in addition to a fast speed and large memory, the board also has a small form factor while still including 64 GPIO pins. Quickly responding electronics allowed for a well-tuned controller.

Ideally, a controller is tuned under the conditions it will normally operate in, but in this case the device needed to be fully tuned and operational before being given to the end-user. In

order to facilitate benchtop tuning of the controller, anthropometric data from Erdmann was used for the radius of gyration about the longitudinal axis and data from Dempster via Winter was used for segment weight distributions in order to calculate an equivalent moment of inertia about the longitudinal axis I_{zz} for a 200-lb, 5-ft 9-in tall person [17]–[19]. A 200-lb weight was chosen as that is the approximate max weight that the TAP device should be able to support, and a height of 5 ft 9 in was chosen as that is the average American male height according to the National Center for Health Statistics [20]. The thigh and shank segments' I_{zz} on the prosthesis side were considered to have the most effect on the device. Moment of inertia calculations were done using MATLAB (The MathWorks Inc., MA, USA) leading to a desired I_{zz} of 0.0779 kg-m^2. That value was used as a guide for creating a CAD model in Onshape (Onshape Inc., MA, USA). Miscellaneous parts from the CLiMB machine shop were used for convenience, leading to a design based around 80/20 aluminum framing (Part No. 40-4040) and a thin-walled aluminum pipe. Before any material was cut, the lengths of each part were changed to reasonable dimensions in a CAD assembly to reach the desired equivalent I_{zz}. The resulting assembly and experimental setup can be seen in Figure 3.1 below. The main goal with this experimental setup was to develop the controller as much as possible with hardware-in-the-loop tuning before anyone stood on it. The main shortcoming of this setup is that it does not take into account body weight during the gait cycle. In particular, body weight as seen by a force plate in the ground will fluctuate throughout stance phase.

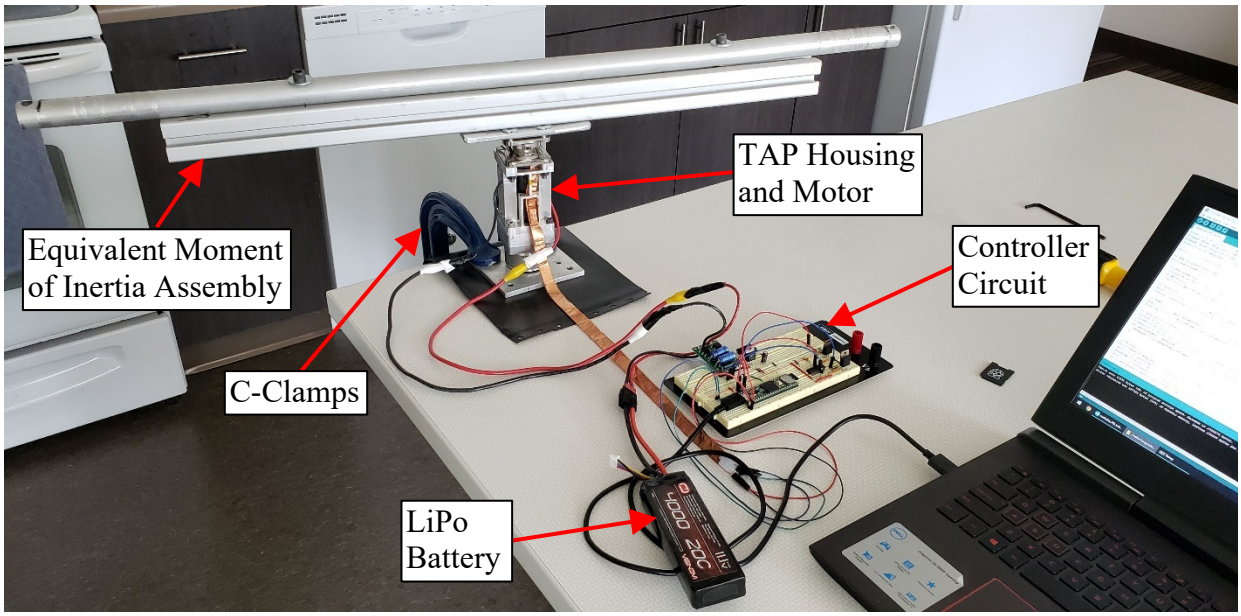

Figure 3.1 The experimental setup for initial tuning of the TAP's controller with the equivalent moment of inertia assembly.

The controller techniques used in initial development of the controller were a combination of Ziegler-Nichols tuning and manual tuning heuristics. A side goal here was the continual development of the code used to implement the controller schema. During tuning, the following data was recorded on a microSD card: time, controller setpoint, motor position, and PWM command signal. This data was then processed in MATLAB for immediate feedback on controller performance. This hardware-in-the-loop tuning combined with rapid feedback allowed the gains to be tuned quickly and incrementally.

The three tuning regimes used to develop the controller were step responses, sinusoidal tracking, and gait lab data tracking. At first a step response was used to tune the controller to respond quick enough to initial contact events, i.e., heel strikes (HS). Initial guidelines for tuning were a quick rise time with minimal overshoot. A step response setpoint of 5.625° (360°/64) was chosen as an approximate upper bound for the range of motion the TAP will have to rotate in practice based on existing ankle sagittal angle curves [3]. A setpoint of 5.625° (360°/64) was

chosen to keep the value as a multiple of one full rotation for ease of conceptualization. Sinusoidal tracking was then used to tune the controller to a simple dynamic response. Dynamic tracking is important after initial contact and through to toe off (TO). Moving back and forth between these two regimes allowed for a response that did not overly compromise either the step or tracking responses. As a final tuning regime, prosthetic pylon-ankle angle data in the sagittal plane previously gathered at the CLiMB gait lab was used to check the response of the controller using the previously derived PID gains of $K_p = 6$, $K_i = 3$, and $K_d = 0.8$ with a coupling ratio of 1:2 to scale to original signal. The performance results of all three regimes are shown in Figures 3.2, 3.3, and 3.4 below. Now that the gains were all at reasonable values for this experimental setup, the next steps would to develop the TAP using the strain gauges and assemble the device as per Figures 2.2 through 2.5.

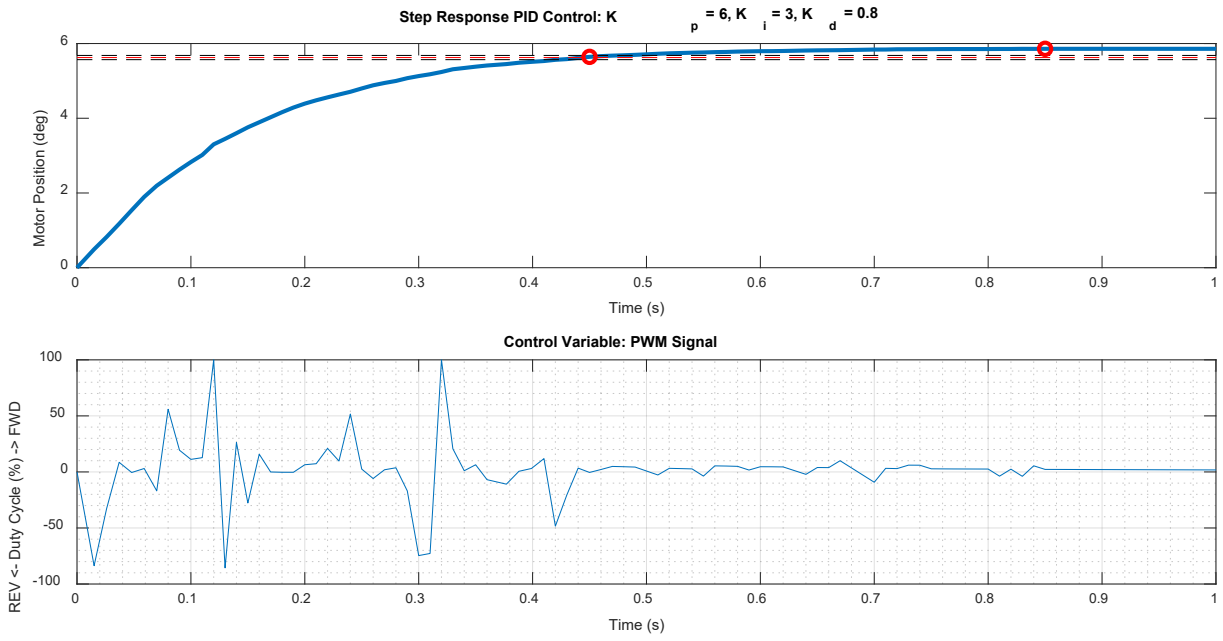

Figure 3.2 Benchtop step response performance using the experimental setup shown in Figure 3.1. From left to right the red circles correspond to a rise time of 0.45 s at 5.64° from 0°, an overshoot of 5.86° at 0.85 s, and (off the plot) a settling time of 5.06 s at 5.68° with a steady-state error of -0.02°.

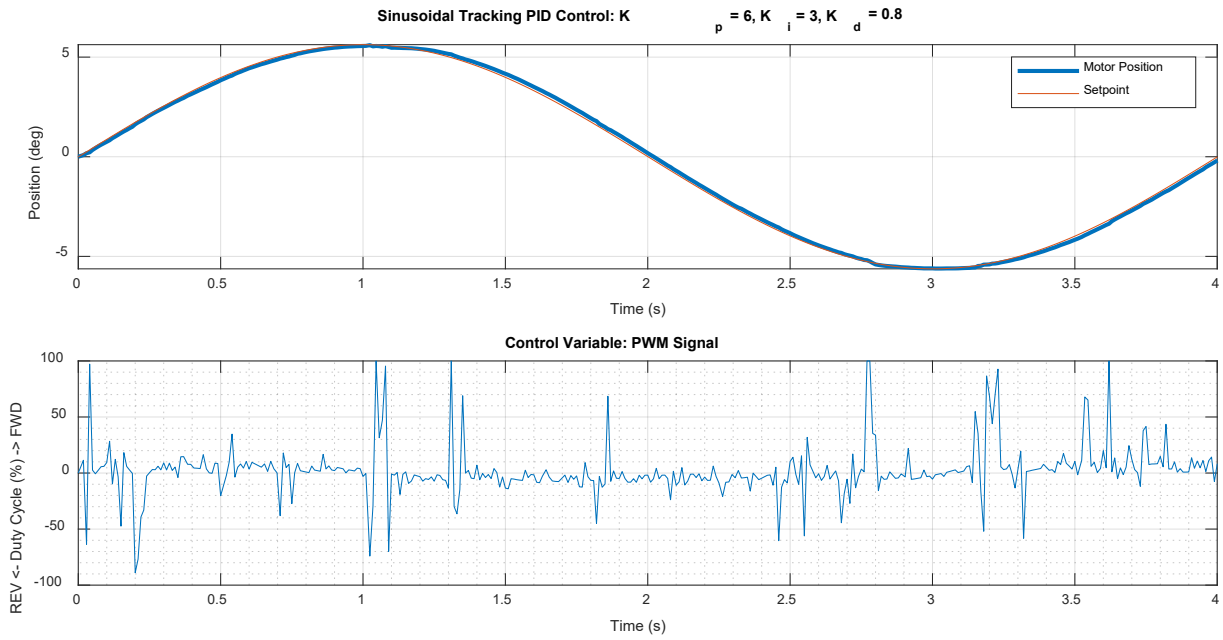

Figure 3.3 Benchtop sinusoidal tracking performance using the experimental setup shown in Figure 3.1. The RMSE is 0.141°.

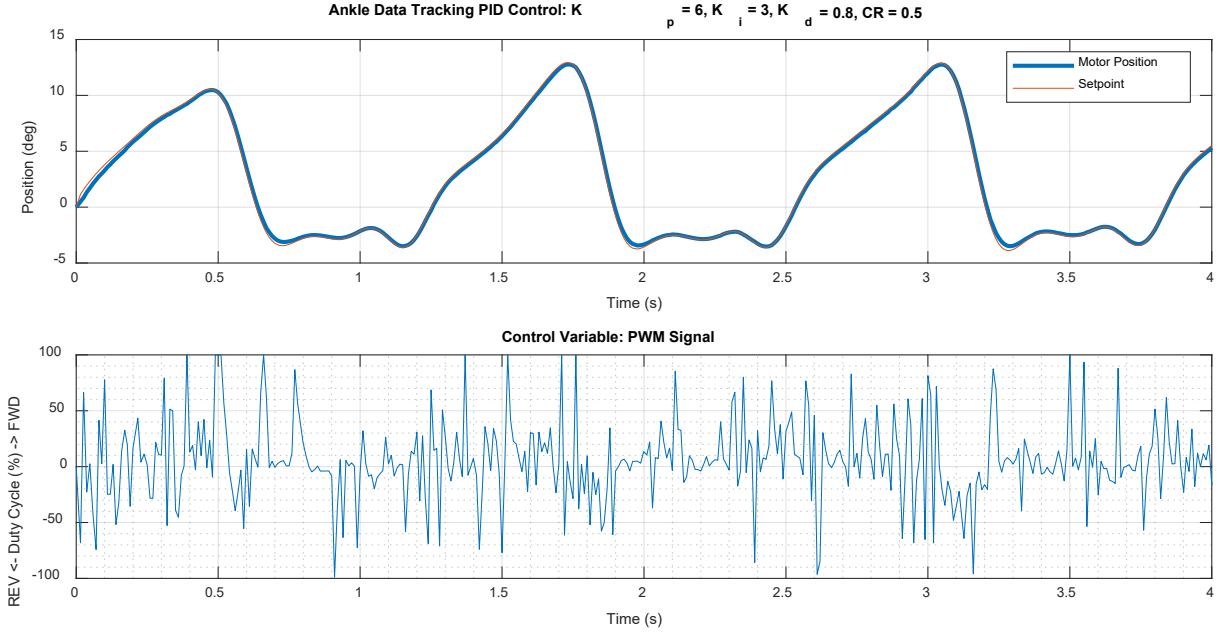

Figure 3.4 Benchtop prosthetic pylon-ankle sagittal angle data tracking performance using the experimental setup shown in Figure 3.1. The RMSE is 0.228°. The CR of 1:2 used here to scale the original data is the largest CR giving the largest range of motion to control over.

3.2 Sensor Mapping

The strain gauges installed on the TAP were used as an approximate, indirect measurement of the prosthetic foot's nonexistent sagittal ankle angle. This mapping from strain to degrees was constructed using Vicon's motion capture system (Oxford Metrics, Oxford, UK) synced with the TAP's electronics. A prosthetic foot actuator (Figure 3.5) was constructed out of 80/20 and a pyramid adapter to help bend the prosthetic foot through the gait cycle in lieu of a person standing on the foot itself. Passive reflective markers were used to model the shank and foot segments in Vicon. Vicon's sync out feature was used to match up the 100-Hz sampling rates of Vicon and the TAP.

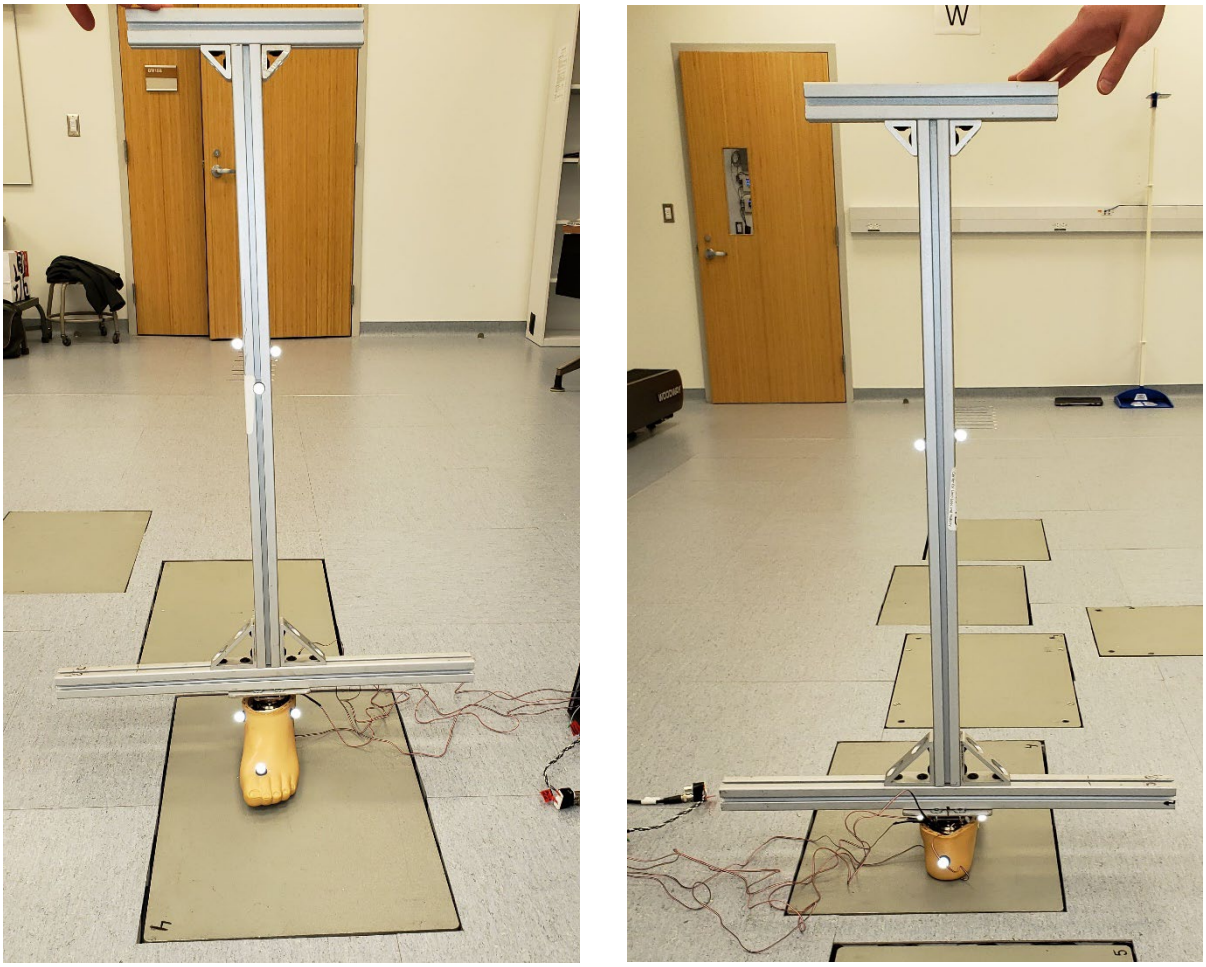

Figure 3.5 The prosthetic foot adapter setup with motion capture markers placed to model the shank and foot using Vicon.

Once the motion capture and strain gage data were gathered using the above setup, Visual 3D (C-Motion, Germantown, MD, USA) was used to process the motion capture data and then MATLAB was used to combine each data set into a corresponding mapping. Figure 3.6 shows the linear mapping for each of the four strain gauges. Linear fits were used to average together the minimum hysteresis seen by the strain gauges in the carbon fiber deflections. Multiple trials of data were collected, and the linear best-fit slopes were averaged together. Table 3.1 shows the slopes used for a category 5, size 25 Össur Low-Profile Vari-Flex foot. Combined with the CR this gave an indirect mapping from strain values to transverse plane angles.

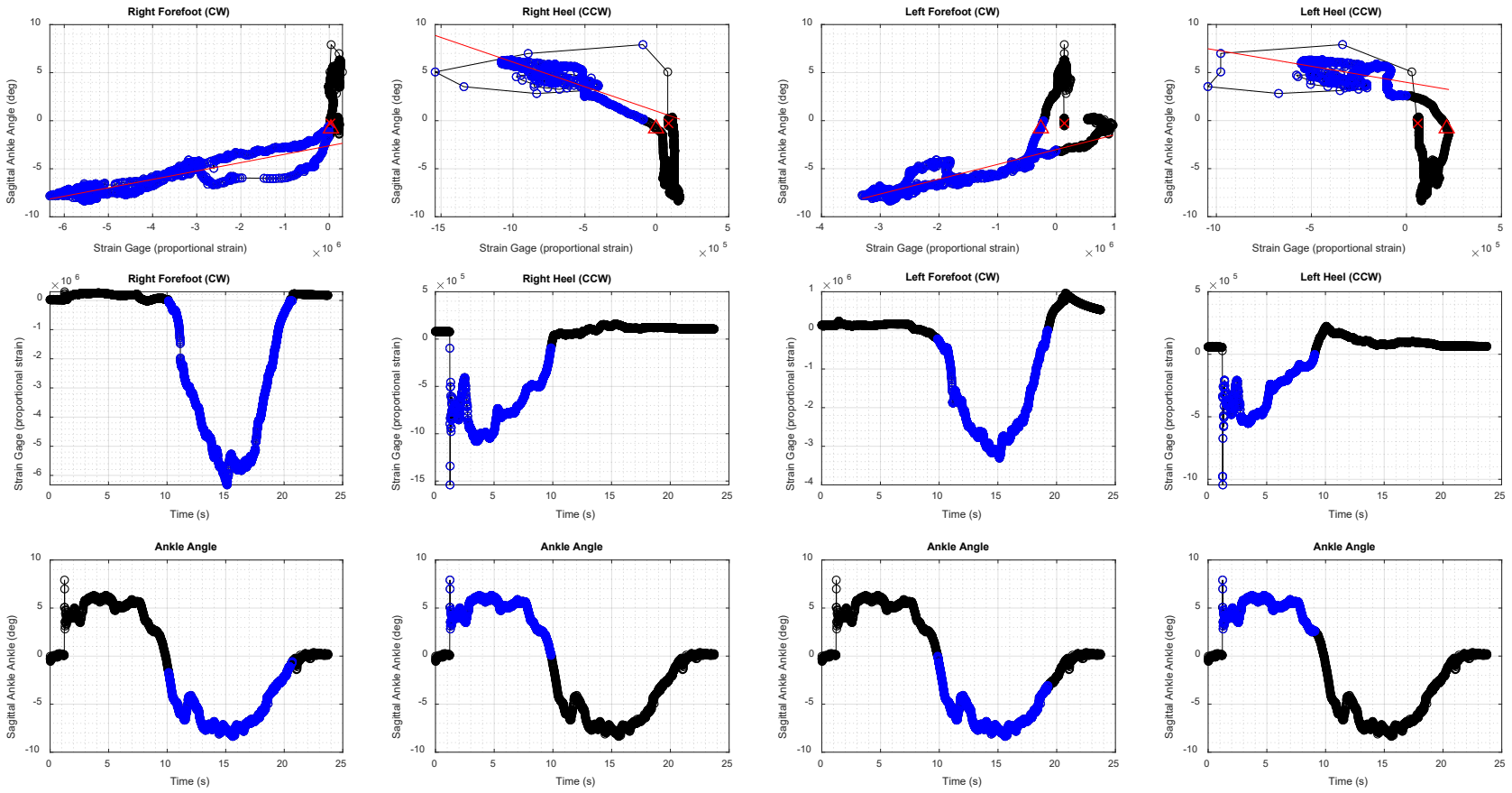

Figure 3.6 Strain gage and motion capture calibration curves for a category 5 size 25 Össur Low-Profile Vari-Flex foot. The top row of plots shows the red linear best fit line used to calculate the strain to angle mapping. The middle row of plots shows the recorded strain gage values by the TAP. The bottom row of plots shows the recorded motion capture derived ankle angle. Blue corresponds to the moments that specific strain gage was compressed below a predefined threshold level, and black corresponds to moments of gage inactivity above the same pre-defined threshold. CW and CCW are clockwise and counterclockwise, respectively, where the red X denotes the start of the hysteresis and the red triangle helps guide the direction of hysteresis on the plot.

Table 3.1 Linear slopes for a category 5, size 25 Össur Low-Profile Vari-Flex foot.

Prosthetic Foot Region	Linear Slope (degree / proportional strain)
Left Heel	$-2.264553 * 10^{-6}$
Right Heel	$-5.013686 * 10^{-6}$
Left Forefoot	$1.488507 * 10^{-6}$
Right Forefoot	$0.8007745 * 10^{-6}$

3.3 Preliminary Testing and Results

Preliminary testing was done by an able-bodied person on the TAP using a modified VacoCast Fit walking boot with an attached custom pyramid adapter mounting plate (Figure 3.7). The boot adapter design was used courtesy of Tristan Gilbert of the Biomechanics and Assistive Technology Laboratory at Vanderbilt University in Nashville, TN. For added safety, a ceiling harness was used for fall protection. The goal of using the boots is to allow an able-bodied person to simulate the kind of walking exhibited by individuals with a lower-limb amputation on a prosthetic device. The testing setup can be seen in Figure 3.7 with the TAP device attached to the left boot while a standard prosthetic foot setup was attached to the right boot. Three testing regimes at a self-selected walking speed were completed with randomized coupling ratios within each regime: straight walking, prosthesis inside circle walking, and prosthesis outside circle walking. Straight walking was the most stable facsimile of the walking patterns exhibited by individuals with lower-limb amputation while using the boots. Relatively normal gait patterns could be achieved at a self-selected walking speed once the user was acclimated to using the boots. Unfortunately, both circle walking regimes exhibited unstable, abnormal gaits. As such the most meaningful results from this preliminary testing came from the straight walking trials.

Custom MATLAB code was used to analyze the output data shown in Figures 3.8 and 3.9. Figure 3.8 presents over time the controller setpoint where the motor is commanded to move to, the encoder feedback giving the true motor position, and the error between the two signals.

The lower subplot shows the pulled motor current used to rotate to the setpoint at that time. Looking at Figure 3.8 it can be concluded that the current state of the PID controller is underperforming. The setpoint does not react quick enough to get a meaningful response time; however, the profile that the controller is creating shows the correct signed angles during each section of stance as can be seen in Figure 3.9. The desired profile is external rotation at HS and internal rotation at TO. Due to compounding errors over time, only the CR of 1:2 had a visibly different angle range, and all other CRs resulted in a similar angle range. This result gave an angle of attack for improving the controller: require swing phase to end at the same, neutral position each cycle before stance begins. A motor current RMS of 6.06 A is a reasonable average current draw for a 60-W DC motor. These preliminary test results show both that benchtop tuning does not take into account fluctuating body weight which led to poor controller tuning and that using the custom adapter boots is a good experimental setup for developing the TAP's software.

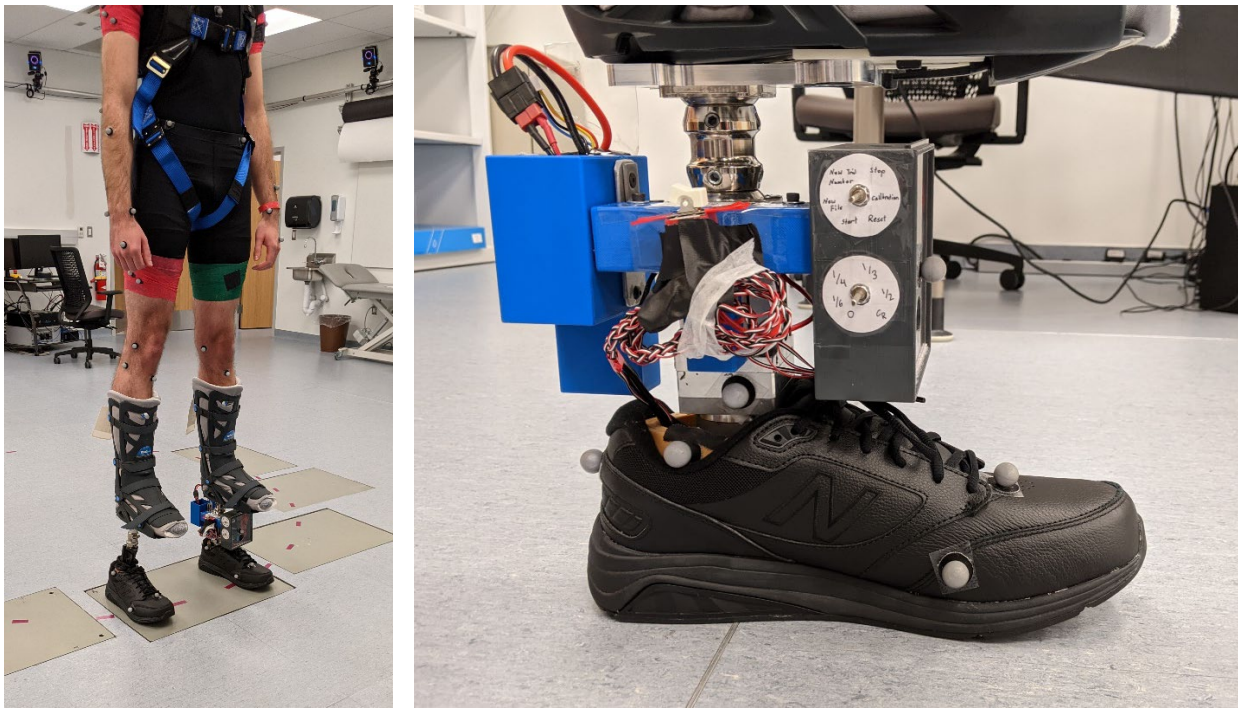

Figure 3.7 Preliminary testing set-up showing the full Vicon plug-in gait marker set (left) and the added TAP device marker set (right).

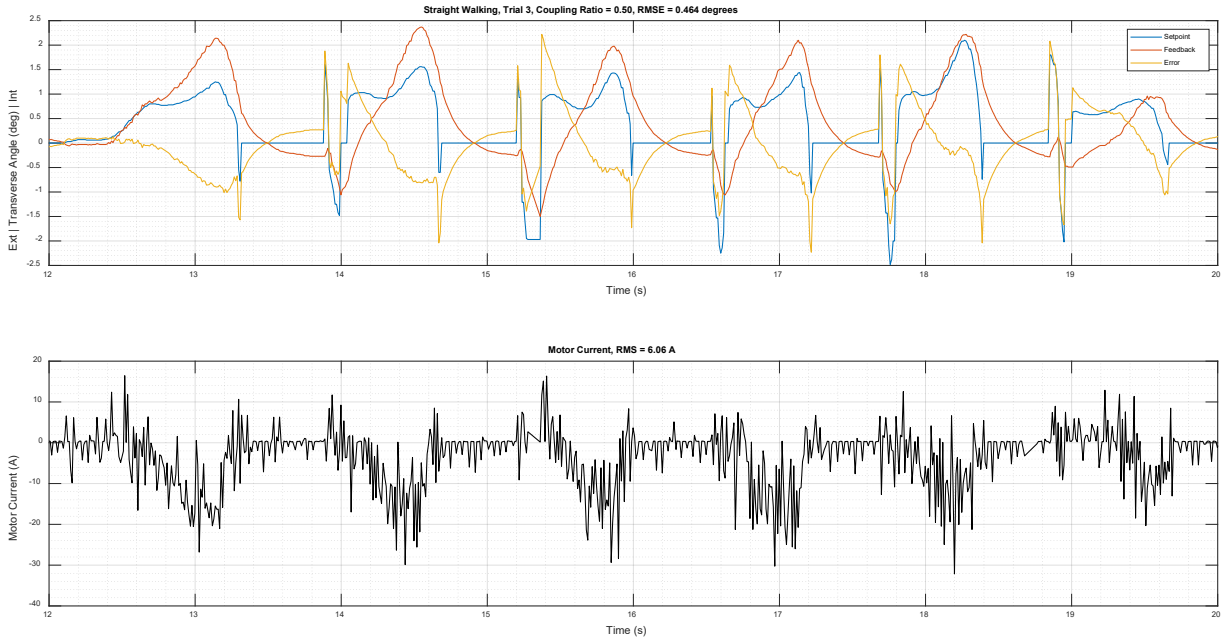

Figure 3.8 Controller performance over time during the straight walking trial for a coupling ratio of 1:2. Feedback here is the motor position given by the encoder.

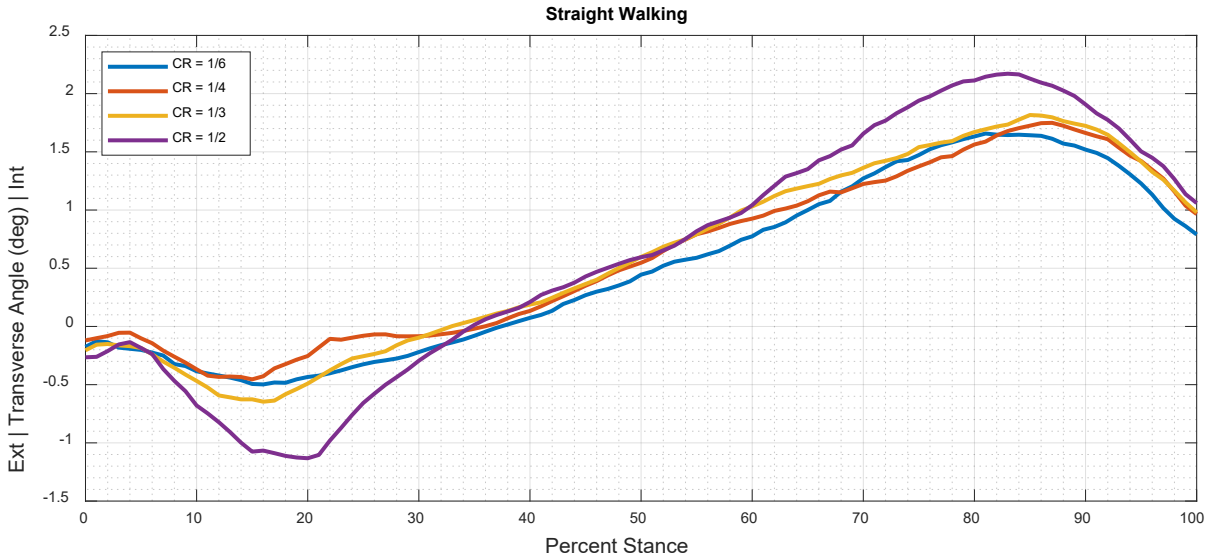

Figure 3.9 These curves were produced by averaging across stance cycles in a single trial then averaging across trials of the same CR. This plot compares how different coupling ratios affected the transverse angle at the ankle while straight walking.

3.4 Treadmill Tuning

The preliminary results made it exceedingly apparent how important applied body weight during stance is to properly tune a controller for the gait cycle. The specific application of body weight during stance can be seen in vertical ground reaction force (GRF) plots showing the characteristic “M” curve [19], [21]. Using the custom boots from preliminary testing, a harnessed able-bodied person was able to walk on the boots with the TAP device over a treadmill (Figure 3.10). The treadmill allowed for much greater control of walking speed and allowed a person to traverse much greater distances compared to the overground distance in the gait lab. A benefit of walking greater distances is an increased amount of steady-state walking cycles for analysis.

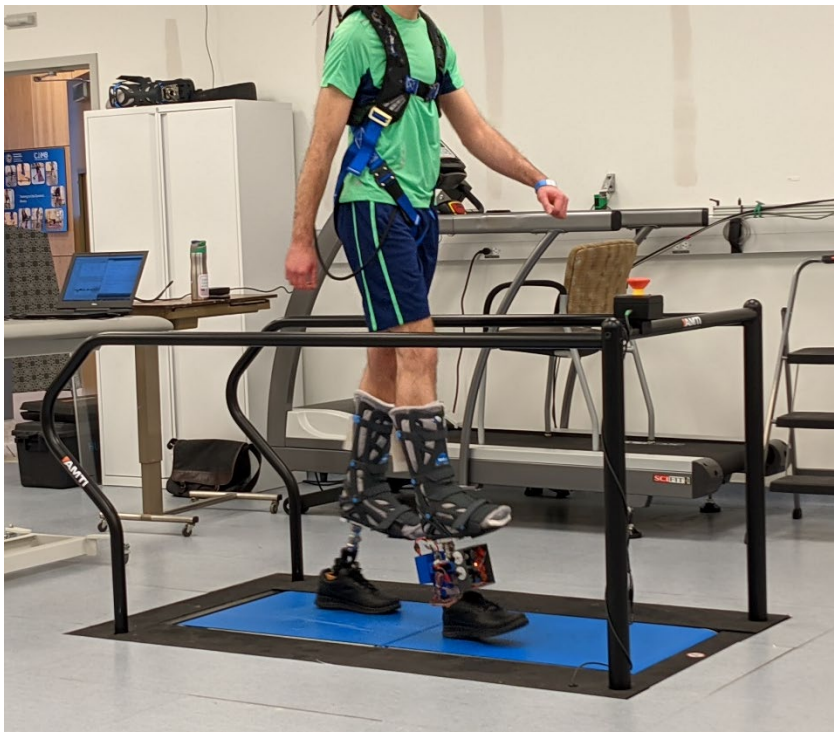

Figure 3.10 Able-bodied walking over a treadmill on the TAP device with custom boots.

Revising the conclusions drawn from Figure 3.8, a necessary step is improving the device's ability to return to a neutral position during swing before the start of the following stance cycle. During swing the TAP has a mechanically-free end which can rotate without any reactive GRFs. The controller is free to use the entire time period between TO and HS to return to a neutral position by the start of the following stance phase. Using gain scheduling to segment the gait cycle between stance and swing, the gains for swing phase were tuned to be step response focused. Figure 3.11 shows the step response for a 1° step using the PD gains shown in Table 3.2 below under swing phase. Over multiple steady state cycles, it was calculated that the average swing phase was lasting anywhere from approximately 200 to 300 ms. Due to the nonlinear nature of passive motor friction being controlled by a linear controller, the step responses from tuning were achieving settling times from around 180 to 300 ms, which is an acceptable range for this application.

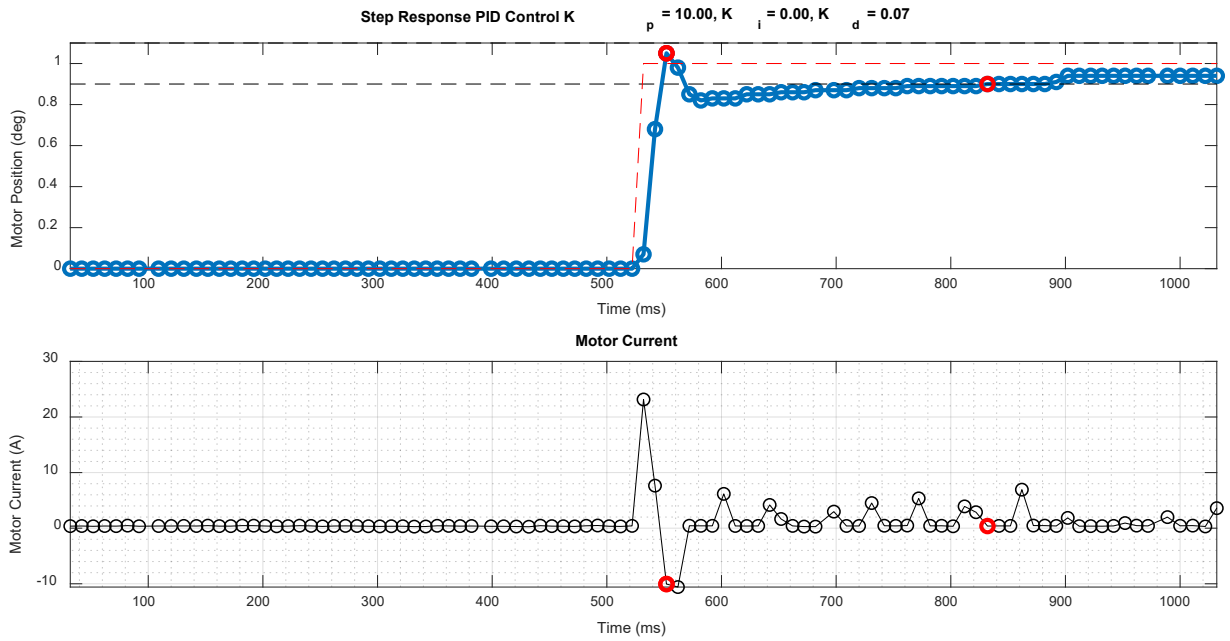

Figure 3.11 Swing phase step response. From left to right the red circles are a rise time of 20 ms at 1.05°, (overlapping with rise time) overshoot of 1.05° at 20 ms, and a settling time of 300 ms achieved at 0.9° which is 0.1° below the setpoint.

The motor current plot in Figure 3.8 shows that there is a large amount of noise being added to the control variable, especially during stance. Looking at the way the PID controller is calculated in practice, the derivative term often considerably amplifies measured signal noise. To filter out the derivative term noise, a simple cumulative moving average filter was applied to this term. Directly comparing the motor current plots shown on Figures 3.8 and 3.12, there is a significant decrease in control variable noise.

The following phases to be tuned were from early to mid-stance and then from mid-stance to late stance. In early stance the dominant force is the weight acceptance GRF. This means that the initial response at HS needs to have a strong, proportional gain step response with less of a time and need for a large integral gain compared to late stance. Mid-stance through late stance deals with rollover and push-off. Rollover is a period where the GRF decreases relative to during weight acceptance so at this moment there is not as much a need for a strong, proportional

gain. The GRF rapidly increases in value as push-off is approached. This means that there is a large need to correct for error from applied external forces leading to a larger integral gain compared to early stance. The final gains for each gait cycle phase are summarized in Table 3.2 below. These gains were as far as an able-bodied user could take this controller using custom adapter boots. This is because body weight is so important to the controller design that either someone needs to walk on the device with custom boots or a gait simulator that can simulate GRFs would need to be used to properly tune and debug the controller.

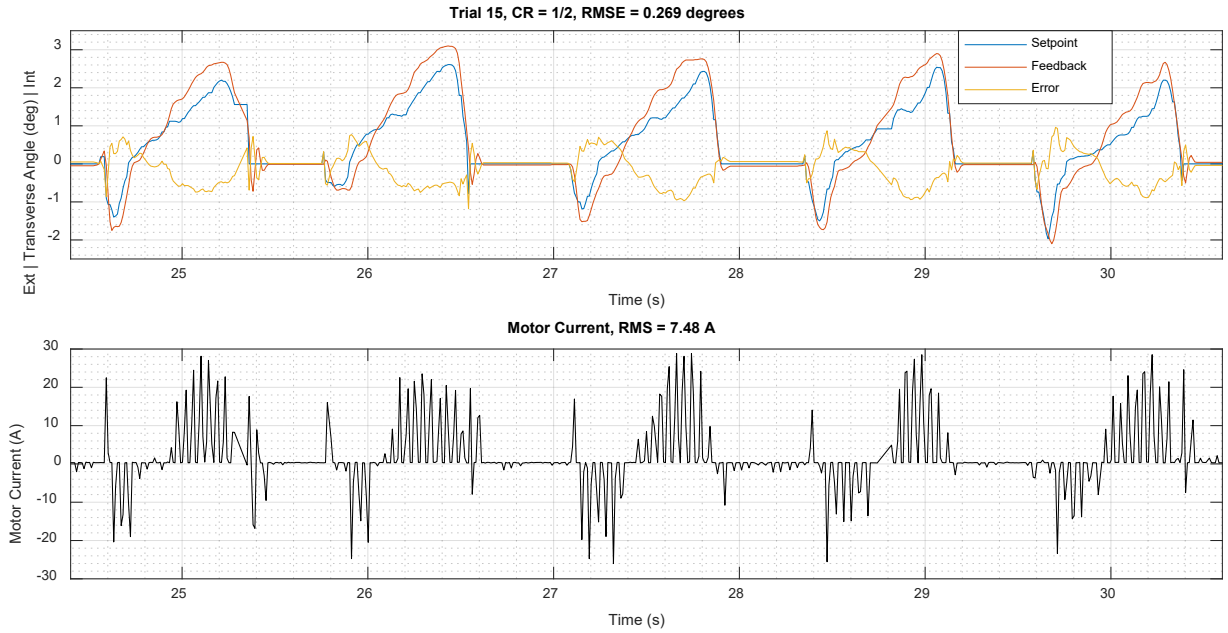

Figure 3.12 Controller performance for the gains developed while walking over the treadmill.

Table 3.2 The scheduled gains for each major phase of the gait cycle.

	Swing Phase	Early to Mid-Stance	Mid-Stance to Late Stance
K_p	10	6	5.5
K_i	0	3	4
K_d	0.07	0.85	0.85

Chapter 4:
Human Subject Testing

Three males with transtibial amputation used the TAP to walk under each CR condition for three different walking regimes: straight walking, prosthesis inside circle walking, and prosthesis outside circle walking. This study had two main hypotheses for each walking regime: (1) there exists a CR that minimizes peak transverse-plane moment and (2) there exists a CR that maximizes user satisfaction. Data was collected using the TAP, passive motion capture markers, and force plates. After collecting enough data for each CR condition, participants were asked to rate their satisfaction level using a socket comfort score on a scale from 0 to 10. Data was analyzed using Visual 3D and MATLAB. Repeated measures ANOVA statistics were calculated using MATLAB's statistics toolbox. Specific points of interest during stance were statistically analyzed to detect if there were any significant differences. The goal being that joint angles, joint powers, and GRFs were unchanged between CRs while transverse torques and socket comfort scores were significantly changed.

4.1 Methods

Three males with transtibial amputations provided informed consent to participate in this IRB-approved study. The mean age was 61 years (±7.9 years) with a mean body mass of 85.3 kg (±3.5 kg) and a mean height of 1.76 m (±0.1 m). All participants met the following inclusion criteria:

1. Has a unilateral transtibial amputation
2. Has been fit with a prosthesis and used it for at least 6 months
3. Has worn the prosthesis for 4 or more hours on average per day

4. Has a prescribed prosthesis that can accommodate fitment of the study prosthetic components to be tested
5. Has no current skin irritation or injury on residual limb
6. Has no osteoarthritis, injury, or pain that interferes with walking ability

All participants wore their own socket, linear, and socks. Prior to each participant's first visit, their prosthetic foot size and category were determined based on their shoe size and weight. Only Össur's low-profile Vari-Flex prosthetic feet were attached to the TAP to keep a minimum build height clearance for varying residual limb lengths. Table 4.1 shows the details of each participant's amputation type and prosthetic components. Self-selected walking speeds for straight walking and circle walking were recorded with their prescribed prosthesis before fitting the TAP. These speeds would later be used as guidelines for keeping walking speed consistent between trials.

Table 4.1 Prosthetic components used. PTB = Patellar Tendon Bearing, TSB = Toral Surface Bearing, LP = Low-Profile, Cat = Category, NR = Not Recorded

Subject	Socket	Liner	Suspension	Pylon / Adapter	Prescribed Foot	Study Foot	Socks
1	Hybrid PTB	ALPS 26	Pin-lock	Standard Rigid	College Park Tru Step, Size 25	LP Vari-Flex Cat 5, Size 25	1 ply
2	TSB	Ohio Willow Wood Alpha Silicone	Pin-lock	Össur Torsion Shock Absorbing	Össur Pro-Flex XC Torsion	LP Vari-Flex Cat 5, Size 25	NR
3	Hybrid PTB	Ohio Willow Wood Alpha Classic	Pin-lock	Standard Rigid	Fillauer All-Pro	LP Vari-Flex Cat 5, Size 29	3 ply

Table 4.2 Participant personal information and transtibial etiology.

Subject	Age	Height (m)	Weight (kg)	Amputation Cause
1	58	1.68	83.8	Trauma
2	55	1.75	89.3	Infection
3	70	1.86	82.8	Trauma

Once the participant was fitted with tight fitting clothing and the TAP was properly fitted and aligned by a prosthetist, reflective motion capture markers were applied to their body. A center-specific marker set was used in addition to the standard full body Vicon Plug-In Gait marker set. The additional markers were placed bilaterally for better tracking and model building on the first and fifth metatarsal heads, medial malleolus, medial knee, medial elbow, fibular head, and tibial tuberosity. Additional clusters of four markers on rigid bases were placed bilaterally on the upper arm and thigh segments. Additional TAP-specific markers were added to the anterior and posterior faces of the device as well as the medial and lateral base of the motor housing as seen in Figure 3.7. The additional TAP markers were used to validate the recorded device transverse rotation. Gait kinematics were collected using sixteen Vantage V8 cameras operating at a sampling rate of 100 Hz to match the TAP sample rate. GRFs and moments were collected using eight AMTI force plates (AMTI, Watertown, MA) operating at a sampling rate of 2000 Hz. Height, mass, and anatomical measurements were recorded according to the Vicon requirements for static and dynamical modeling. In addition to the Vicon static trial, a TAP calibration was done to adjust the strain gage baseline reference values per each participant's body mass. During TAP calibration, the participant was instructed to stand still to not induce any artifacts while the strain gauge values were being averaged together.

After setup, participants walked across force plates embedded in the floor both in a straight line and in both directions around a circle with a 1-m radius (Figure 4.1). Before each test, participants were given time to walk across the plates both to develop a natural cadence as well as adjust the starting position to better make full contact with the force plates during natural gait. The 1-m radius circle was marked with a dashed line on the floor. The three walking regimes are labeled going forward as Straight (ST) walking, Prosthesis Inside (PI) circle

walking, and Prosthesis Outside (PO) circle walking. Participants performed at least ten trials for each walking regime, resulting in at least two good trials for each of the five CRs. A good trial was defined as having at least one good force plate strike with each foot. Trials that did not meet this requirement were repeated until a good trial was achieved. Good force plate strikes were defined as steps with one foot entirely on a plate from HS to with no interference from the other foot striking the same plate.

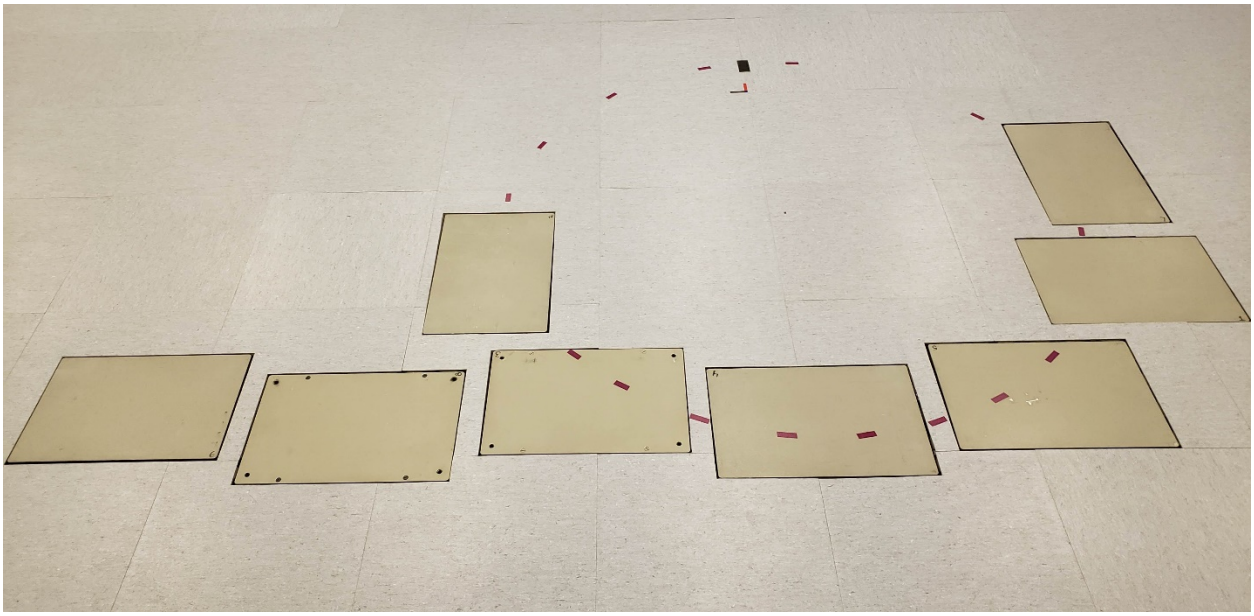

Figure 4.1 CLiMB gait lab force plates setup for both straight walking and 1-m circle walking.

Five CR configurations were used for the TAP. The order of the three testing regimes were randomized, and within each testing regime the CR order was also randomized. Between each CR change the participant was asked for a socket comfort score for the current CR setting. The socket comfort score is presented as follows: On a 0 – 10 scale, if 0 represents the most uncomfortable socket fit you can imagine, and 10 represents the most comfortable socket fit, how would you score the comfort of the socket fit of your artificial limb at the moment? All the torque data, motion capture data, force plate data, and socket comfort scores for a single testing regime were collected before moving on to the next regime.

4.2 Data Analysis

The data recorded on-board the TAP was processed using MATLAB independently from the motion capture marker data. The controller's setpoint for motor rotation changed during the gait cycle depending on how much the prosthetic foot was bending. Of note, during swing the foot was no longer bent under body weight, so the setpoint was set to a neutral position of zero. This allowed gait phases to be detected based on if the prosthetic foot was being bent or not. Segmenting out these phases into stance and swing, the stance cycles were normalized into percent stance and then averaged together across multiple cycles and like trials. Transverse ankle angle was recorded using the built-in motor encoder. Shank torque was interpreted as applied motor torque, which is directly proportional to applied motor current scaled by the motor torque constant taken from the motor's data sheet.

The motion capture marker data was processed in Visual 3D to calculate gait kinematics, kinetics, and gait event timings. Marker positions were filtered using a bidirectional Butterworth filter at a 6-Hz cutoff frequency. Force plate outputs were filtered with a bidirectional Butterworth filter with a 25-Hz cutoff frequency. Bilateral sagittal and transverse joint angles and joint powers were calculated and compared against baseline curves. Coordinate system transformations for GRFs and joint powers were done in Visual 3D for all trials. These coordinate systems were transformed to the participant's torso coordinate system to keep calculations in line with the direction of progression. In the absence of an ankle joint in the participants' prosthetic systems, the total power of the below-knee structures was calculated using Takahashi's unified deformable (UD) segment model [22]. The benefit of using this method is that it does not require defining an ankle joint or foot segment. The method instead

models all structures distal to the knee as a UD segment that can generate, store, dissipate, and/or return energy.

Lower-limb kinematics and kinetics were analyzed in Visual 3D to show that the TAP did not affect anything outside of its designed effect. Absolute motor torque was analyzed in MATLAB. The statistical hypotheses being a significant change in socket torque and socket comfort score from an actively changing transverse ankle angle and an insignificant change in gross kinematics and kinetics. Repeated measures ANOVAs (rANOVA) were calculated in MATLAB using the statistics toolbox for joint angles, joint powers, GRFs, UD powers, and absolute motor torques for each walking condition and coupling ratio. A level of significance of $p < 0.05$ was used for all comparisons. Due to the low number of initial participants (n=3), insufficient statistical power to draw conclusions is expected for all metrics; however, the rANOVA analyses are setup for future analyses with the enrollment of additional participants. In this thesis, no final statistical conclusions will be drawn outside of discussing trends. Stance cycles were exported from Visual 3D to MATLAB. Joint kinematics during full extension for the hip joint and weight acceptance for the knee joint were chosen as the discretized points for statistical analysis. Discretized points during push-off for joint kinetics were chosen according to Winter and Sienko [23] to compare. These points of interest are labeled as H3 for the hip joint and K3 for the knee joint during push-off. GRFs during weight acceptance were chosen at the discretized points of interest to compare. Maximum, absolute motor torques were chosen to compare as a metric of motor performance and proportional socket torque. These reference points were used as the repeated measure in the rANOVA analysis. Once in MATLAB the data was organized into formatted tables to run descriptive and repeated measures statistics. A balanced design was achieved by truncating the number of values across all CRs to the lowest

number of values across all participants. If Mauchly's Test of Sphericity was rejected, then the adjusted Greenhouse-Geisser p-value was reported. If it is not rejected, then the unadjusted p-value was reported. Any significant interactions were explored further using estimated marginal means for multiple comparisons.

4.3 Inertial Modeling

Body specific inertial parameters are needed to propagate GRFs up the kinematic chain to determine joint powers. All body segments except the prosthesis side shank and foot used masses proportional to an adjusted total body mass, *ABM*. The adjusted mass was derived using prosthesis mass distribution estimates from Smith [24] to estimate a replacement mass for the amputated limb. By taking apart and measuring components of prosthetic limbs, Smith estimated that 66% of the total prosthesis mass was distributed in the prosthetic socket and 34% was distributed to the foot [24]. *ABM* is calculated via a mass balance in kilograms as follows:

$$ABM = M - 2M_{shoe} - M_{pfoot} - M_{pshank} + f_{foot}ABM + f_{shank}ABM$$

Equation 4.1 Mass balance relating Adjusted Body Mass to measured body mass.

where *M* is measured body mass, *M* with a subscript is component mass, and *f* is the fraction of body mass in the subscripted body segment taken from the anthropometric data in Dempster [18]. All values in Equation 1.1 are known except *ABM*. M_{pshank} can be expressed as:

$$M_{pshank} = 0.65 f_{shank} ABM + M_{TAP}$$

Equation 4.2 The mass breakdown of the prosthesis shank segment using [24] for the 65% prosthesis mass distribution in the shank and [18] for f_{shank}.

Solving for *ABM* and substituting Equation 4.2 into Equation 4.1:

$$ABM = \frac{M - 2M_{shoe} - M_{pfoot} - M_{TAP}}{1 - f_{foot} - 0.34 f_{shank}}$$

Equation 4.3 Adjusted Body Mass, *ABM*, calculated from measured values and estimated prosthesis mass distributions.

where f_{foot} is 0.0145 and f_{shank} is 0.0465. A breakdown of prosthesis mass values for participant 1 can be seen Table 4.3 below showing a total prosthesis mass of 2.9 kg. The TAP shank component was the heaviest component at a mass of 1.7 kg. Using Equation 4.3 participant 1, for example, had a measured body mass of 83.8 kg with an adjusted mass of 83.3 kg which is a difference of 459 g.

Table 4.3 A breakdown of prosthesis mass values for participant 1. M_{TAP} is the mass of the TAP with a battery: 1712 g + 256 g = 1968 g.

Part	Mass (g)
Sock	21
32mm Statis Adapter	81
Low-Profile Vari-Flex C5 S25 (M_{pfoot})	207
Cosmesis Size 25	229
Battery	256
Shoe Size 9 (M_{shoe})	405
TAP (without battery)	1712
Total Mass	2911

4.4 Results

TAP motor torque and socket comfort scores were the only study outcomes with the design goal of showing significant changes. Joint kinematics and kinetics were analyzed to show if the TAP had any significant effect. If there are no significant differences found in any gross kinematics and kinetics, then the TAP as an intervention does not cause any undesirable, inefficient gait compensations to use. The initial statistical results presented in this thesis are only generalizable to the study's sample population (n=3) and not to the entire population of individuals with lower-limb amputation.

The TAP motor performed in the transverse plane within a range of -3 to 3 degrees (Figure 4.2). The larger the CR, the larger the angle range produced as designed. In general, the angle range produced for each participant depended on personal walking habits. These habits

could affect how much of their body weight they dedicate to their prosthetic limb during ambulation.

Absolute motor torque was reported instead of signed torque to better characterize the motor's performance independent of rotation direction. Motor torque was interpreted as an indirect measurement of socket torque. Table 4.4 reports the peak motor torques shown in Figure 4.2. Over the entire stance phase, the motor torque while CR = 0 was generally greater in magnitude than any other CR. Figure 4.3 shows the absolute peak torque distributions per CR per unaveraged stance phases for every participant. On average, off-zero CRs had a more consistent motor torque profile when compared to the zero CR. A rANOVA was done on the peak torques for each walking regime. Initial results presented in both Figure 4.3 and Table 4.5 suggest a small CR will minimize socket toque within each walking regime. A linear, increasing trend for ST suggests a small or zero CR will minimize socket torque. A positive quadratic relationship may exist for PI and PO, suggesting a small, nonzero CR will minimize socket torque for turning gait. For both circle walking regimes, a CR of 0 presented a larger mean motor torque compared to 1:6 and 1:4. The socket comfort score for each CR for each walking regime was recorded for each participant on a 0-10 scale. The scores recorded changed minimally if at all for how they felt about their socket's fit with a within-subject standard deviation of less than one across all participants and walking regimes (Figure 4.4). Both results mean that the study hypotheses that there exists a CR that minimizes socket torque and maximizes user satisfaction were both inconclusive for this sample population (n=3).

Figures 4.5 and 4.6 show joint angles and powers, respectively, in the sagittal plane for each walking condition and CR. The point of interest for the hip joint angles was at full extension for both legs, and knee joint angles were analyzed at peak weight acceptance for both

legs. Both the hip and knee joint powers were analyzed at their corresponding H3 and K3 peaks, respectively. The H3 and K3 peaks both occur at push-off. No trends in points of interest during stance were observed within any walking condition (Tables 4.6 and 4.7). Any deviations seen in these plots can most likely be attributed to user-specific walking patterns and/or a lack of a significant number of force plate strikes. For example, the PO non-prosthesis side hip plot in Figure 4.6 shows noisy variations between CRs due to a low number of good force plate strikes to average together.

The GRFs in Figure 4.7 show the vertical and anterior-posterior GRF responses for a participant's prosthesis side. Both GRFs were analyzed during peak weight acceptance. This corresponds to the first peak in the vertical direction and the lower, breaking peak in the direction of progress. There were no trends between CRs within a walking condition (Table 4.8). An observed difference between PO to ST and PI is the slightly increased GRF during weight acceptance. This could be contributed to the prosthesis side needing to not only accept body weight but change the walking direction. The results of the UD analysis are shown in Figure 4.8. The peak at push-off was chosen as the point of interest. There were no trends observed within walking conditions (Table 4.9). Overall, the TAP, therefore, did not appear to affect any gross kinematics and kinetics.

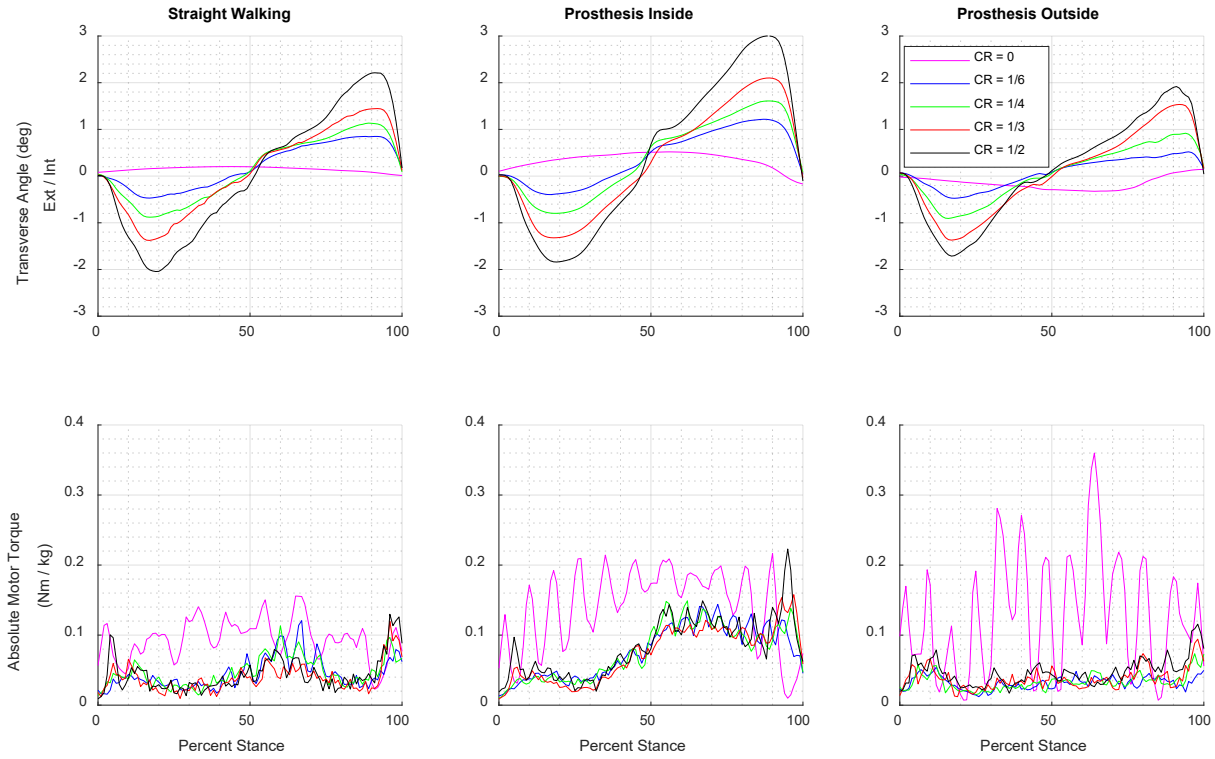

Figure 4.2 Averaged TAP motor angles and absolute torques for each walking condition and CR for participant 2.

Table 4.4 Absolute peak motor torques in Nm/kg corresponding to the plots given in Figure 4.2.

CR	ST	PI	PO
0	0.16	0.22	0.36
1:6	0.12	0.14	0.05
1:4	0.11	0.15	0.07
1:3	0.12	0.16	0.09
1:2	0.13	0.22	0.12

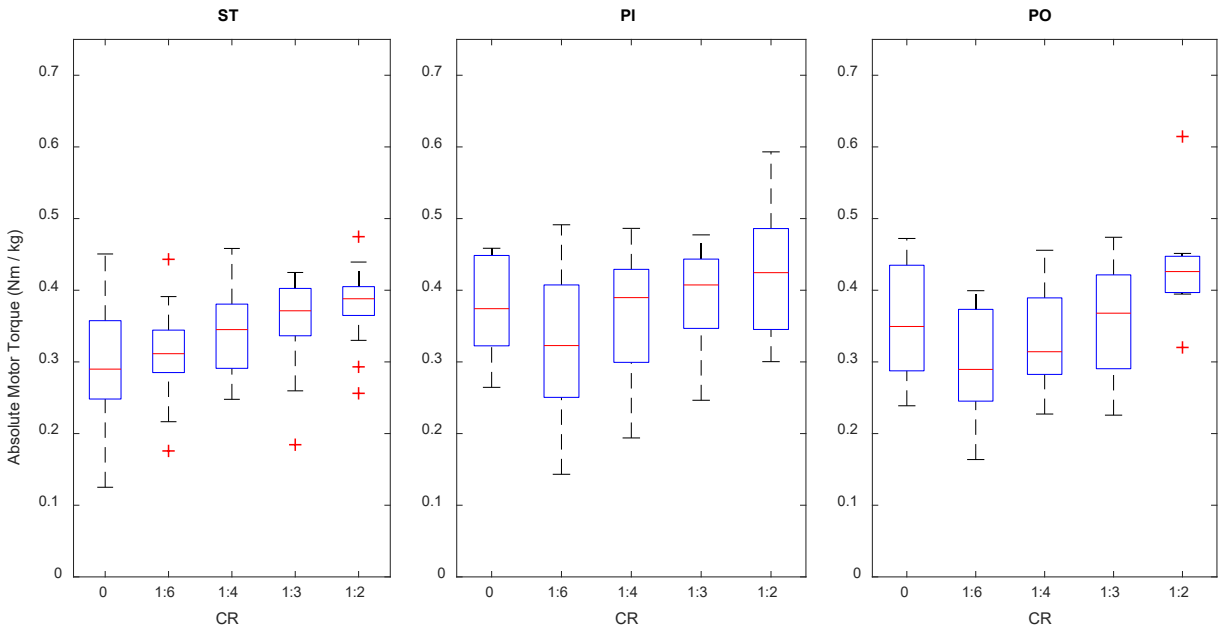

Figure 4.3 Absolute peak motor torques per step for unaveraged stance phases for every participant. Outliers are represented as red pluses.

Table 4.5 Mean (SE) for absolute peak motor torques with associated p-values.

CR	ST	PI	PO
0	0.29 (0.08)	0.38 (0.07)	0.36 (0.09)
1:6	0.31 (0.06)	0.32 (0.11)	0.30 (0.08)
1:4	0.34 (0.05)	0.37 (0.09)	0.34 (0.08)
1:3	0.36 (0.06)	0.40 (0.08)	0.36 (0.09)
1:2	0.38 (0.05)	0.42 (0.09)	0.43 (0.08)
p	0.33	0.24	0.15

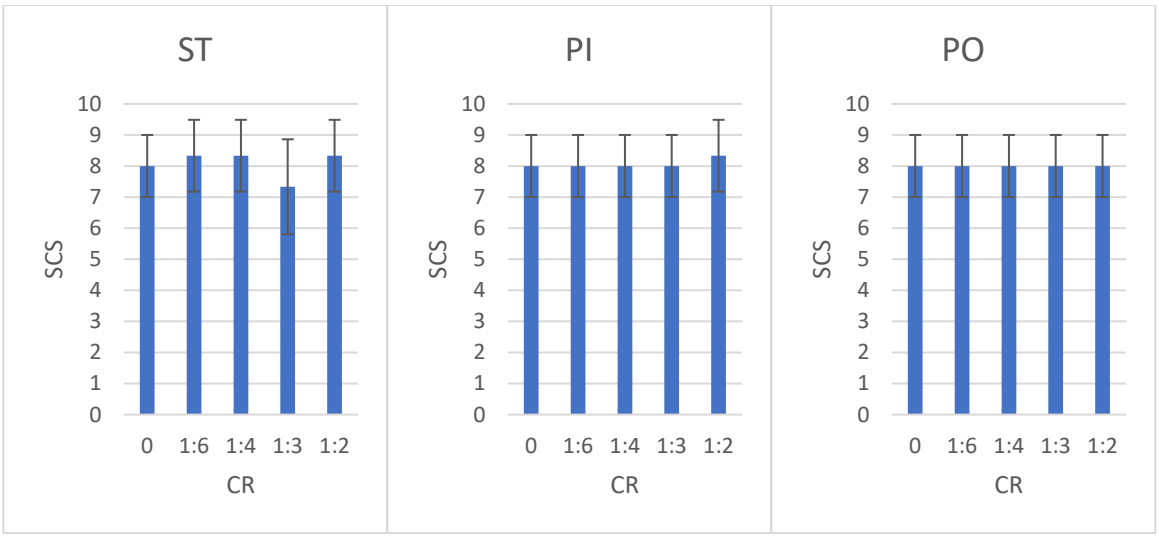

Figure 4.4 Socket Comfort Score (SCS) for each walking regime for each CR showing the study sample (n=3) mean and standard deviation. There are no trends presented between SCS and CR.

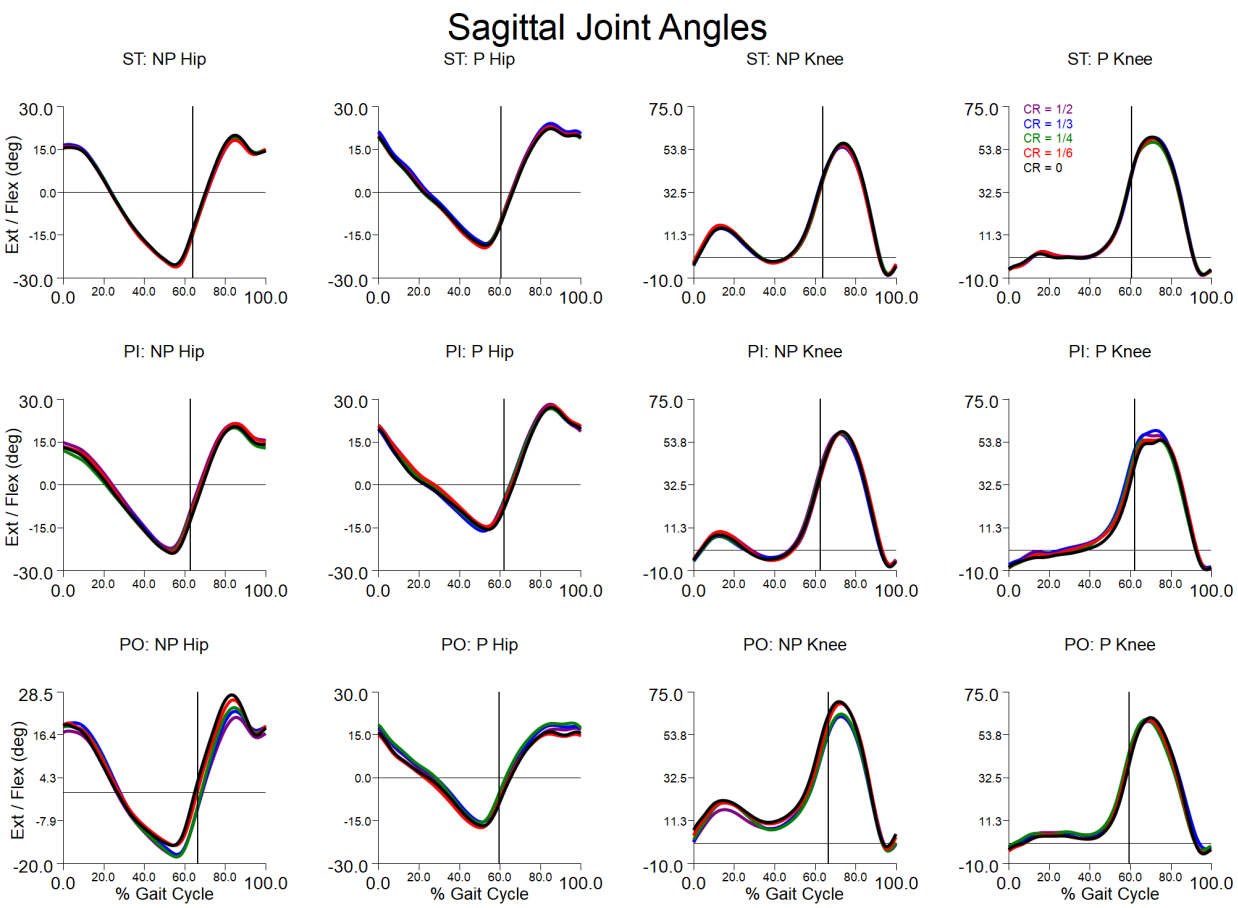

Figure 4.5 Hip and knee sagittal joint angles for ST, PI, and PO walking under each CR condition for participant 2. Joint angles profiles were insensitive to changes in CR. NP = Non-Prosthesis side, P = Prosthesis side.

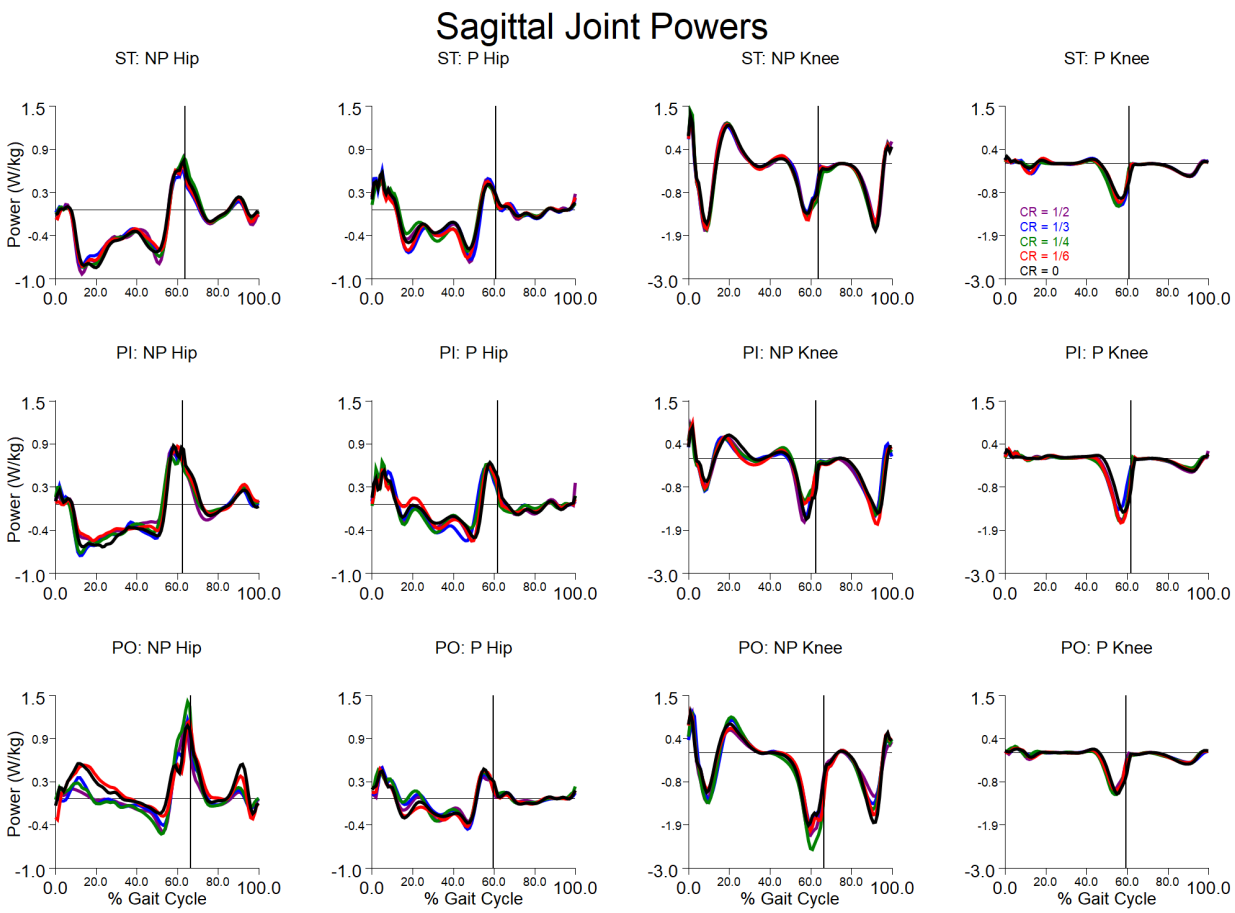

Figure 4.6 Hip and knee sagittal joint powers for ST, PI, and PO walking under each CR condition for participant 2. Joint power profiles were insensitive to changes in CR. NP = Non-Prosthesis side, P = Prosthesis side.

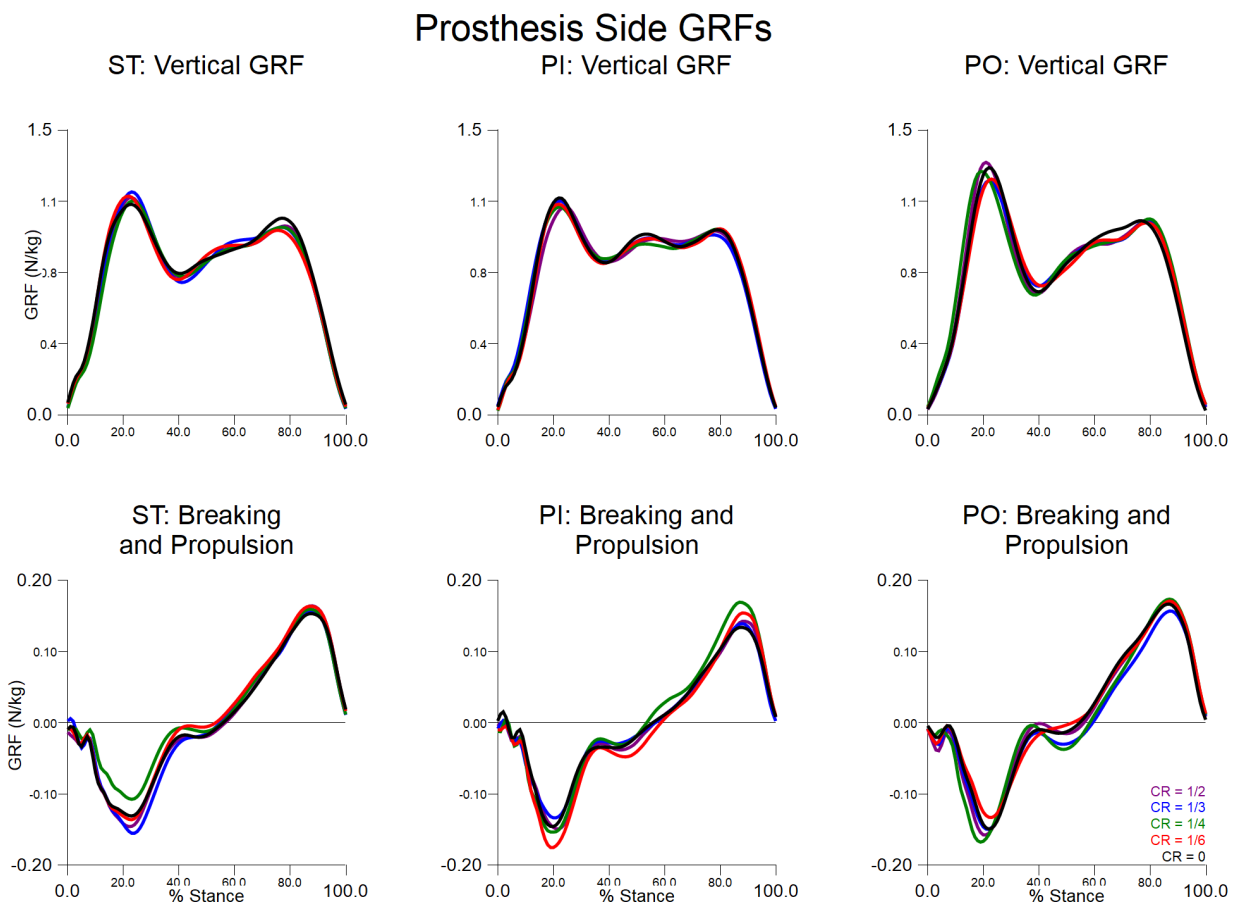

Figure 4.7 Prosthesis side vertical and breaking and propulsive GRFs for participant 2.

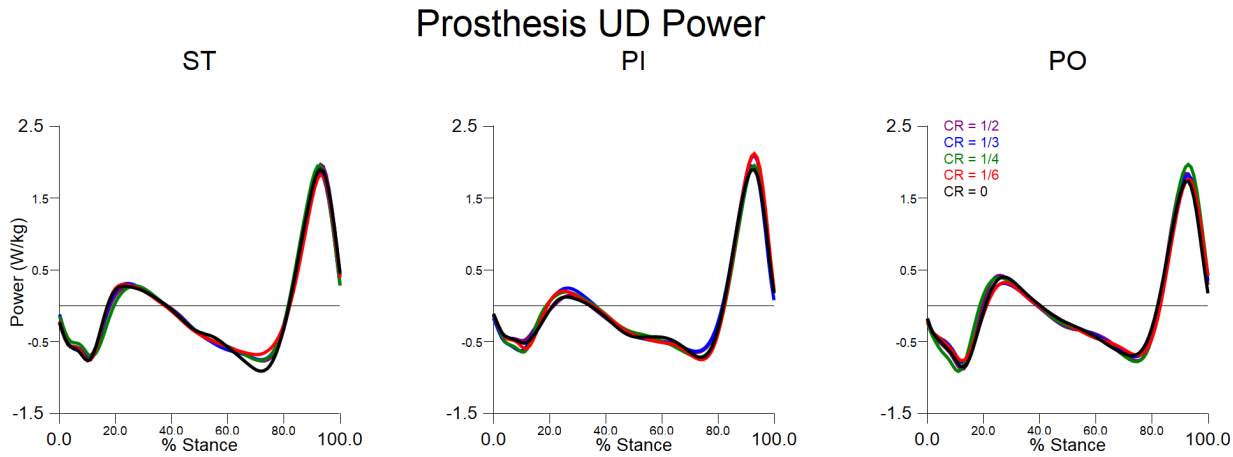

Figure 4.8 Approximated prosthesis power for participant 2 using a unified deformable segment model detailed by Takahashi [22].

Table 4.6 Mean (SE) for sagittal joint angles with associated p-values.

Prosthesis side						
	Hip			Knee		
CR	ST	PI	PO	ST	PI	PO
0	-23.11 (2.69)	-16.14 (3.79)	-15.95 (1.06)	3.05 (0.52)	1.87 (2.78)	3.46 (0.58)
1:6	-22.64 (3.52)	-16.22 (2.33)	-16.66 (0.90)	3.97 (0.07)	4.86 (2.54)	6.67 (1.52)
1:4	-22.24 (3.18)	-15.23 (0.61)	-16.76 (0.71)	4.49 (0.65)	4.76 (4.05)	7.17 (1.99)
1:3	-21.41 (2.29)	-16.39 (1.91)	-17.86 (0.76)	3.19 (1.12)	4.02 (3.17)	5.97 (2.01)
1:2	-20.82 (1.79)	-14.78 (4.25)	-17.05 (0.88)	3.91 (1.39)	2.31 (2.43)	5.90 (2.33)
p	0.32	0.75	0.61	0.39	0.47	0.20
Non-prosthesis side						
	Hip			Knee		
CR	ST	PI	PO	ST	PI	PO
0	-24.28 (1.91)	-16.06 (4.31)	-12.81 (1.37)	11.24 (4.03)	7.84 (1.84)	13.52 (4.56)
1:6	-23.60 (1.52)	-12.09 (4.77)	-17.07 (0.63)	11.54 (3.57)	6.00 (2.19)	13.95 (4.91)
1:4	-23.25 (1.88)	-15.66 (3.76)	-17.39 (0.61)	12.94 (2.69)	8.11 (1.72)	12.54 (3.93)
1:3	-22.56 (2.29)	-15.36 (3.88)	-14.89 (0.83)	11.93 (5.23)	8.14 (3.18)	16.42 (3.26)
1:2	-22.92 (1.70)	-15.16 (3.62)	-15.22 (1.30)	10.83 (4.15)	6.68 (1.55)	13.07 (2.52)
p	0.19	0.26	0.20	0.57	0.51	0.62

Table 4.7 Mean (SE) for sagittal joint powers with associated p-values.

Prosthesis side						
	Hip			Knee		
CR	ST	PI	PO	ST	PI	PO
0	0.72 (0.20)	0.77 (0.05)	0.51 (0.06)	-1.42 (0.29)	-1.23 (0.16)	-0.77 (0.13)
1:6	0.66 (0.19)	0.77 (0.11)	0.45 (0.10)	-1.08 (0.20)	-1.21 (0.24)	-0.74 (0.17)
1:4	0.76 (0.21)	0.86 (0.11)	0.47 (0.11)	-1.36 (0.18)	-1.28 (0.13)	-0.88 (0.16)
1:3	0.64 (0.20)	0.76 (0.12)	0.56 (0.10)	-1.05 (0.15)	-1.28 (0.19)	-0.93 (0.12)
1:2	0.61 (0.18)	0.69 (0.11)	0.46 (0.04)	-1.08 (0.27)	-1.06 (0.28)	-0.83 (0.15)
p	0.14	0.38	0.36	0.28	0.37	0.11
Non-prosthesis side						
	Hip			Knee		
CR	ST	PI	PO	ST	PI	PO
0	1.04 (0.39)	0.78 (0.07)	1.24 (0.07)	-1.30 (0.21)	-1.15 (0.44)	-1.79 (0.10)
1:6	0.97 (0.42)	0.77 (0.08)	1.30 (0.23)	-1.44 (0.48)	-1.27 (0.27)	-1.97 (0.20)
1:4	0.92 (0.30)	0.68 (0.15)	1.15 (0.03)	-1.37 (0.28)	-1.19 (0.32)	-1.61 (0.40)
1:3	0.90 (0.29)	0.66 (0.04)	1.39 (0.08)	-1.33 (0.34)	-0.98 (0.11)	-2.00 (0.56)
1:2	1.01 (0.45)	0.83 (0.04)	1.18 (0.01)	-1.41 (0.48)	-0.87 (0.15)	-1.75 (0.38)
p	0.57	0.48	0.56	0.72	0.43	0.54

Table 4.8 Mean (SE) for GRFs with associated p-values.

	Vertical GRF			Breaking and Propulsive GRFs		
CR	ST	PI	PO	ST	PI	PO
0	1.14 (0.08)	1.05 (0.04)	1.13 (0.11)	-0.15 (0.07)	-0.10 (0.02)	-0.13 (0.04)
1:6	1.14 (0.09)	0.95 (0.09)	1.06 (0.11)	-0.16 (0.08)	-0.12 (0.05)	-0.10 (0.04)
1:4	1.13 (0.08)	1.08 (0.07)	0.98 (0.15)	-0.16 (0.06)	-0.11 (0.04)	-0.11 (0.04)
1:3	1.10 (0.05)	1.04 (0.02)	1.05 (0.09)	-0.13 (0.06)	-0.11 (0.03)	-0.12 (0.03)
1:2	1.08 (0.05)	0.90 (0.14)	1.11 (0.07)	-0.14 (0.06)	-0.10 (0.03)	-0.12 (0.03)
p	0.50	0.30	0.23	0.31	0.65	0.38

Table 4.9 Mean (SE) for UD powers with associated p-values.

CR	ST	PI	PO
0	1.79 (0.28)	1.42 (0.30)	1.34 (0.10)
1:6	1.73 (0.25)	1.62 (0.33)	1.38 (0.38)
1:4	1.71 (0.21)	1.47 (0.17)	1.31 (0.29)
1:3	1.59 (0.27)	1.41 (0.27)	1.44 (0.22)
1:2	1.71 (0.29)	1.42 (0.27)	1.30 (0.21)
p	0.32	0.38	0.83

4.5 Discussion

Several limitations should be considered when interpreting the findings of this study. A small sample size (n=3) directly affects the statistical power, so having more participants should lead a better chance of detecting small differences. A small sample size also means that the results here are not generalizable to the entire population of individuals with lower-limb amputation. Only males have participated in this study also affecting the generalization of results. Future word must ensure recruitment of both males and females.

Although the sample size for this study was small, the rANOVAs were set up to look at points of interest in individual stance phases across all CRs for each subject. The points of interest per stance phase were the repeated measures, and the CRs were the within-subject parameters. To maintain a statistically balanced design, each stance phase metric was aggregated in a table and then each row of metrics was truncated to be the same length. In this manner there were many data points that were ignored because of how the rANOVA is set up. This statistical

setup could affect its ability to detect small differences. An alternative method, such as a linear mixed effects model, could improve the number of data points used in the analysis and increase the chances of detecting small differences.

The TAP is a novel, powered prosthetic device, so it is likely that there would exist an acclimation period when a participant switches from their common, passive prosthetic foot. Wurdeman et al. [25] showed that dynamic balance changes occurred over a period of time for lower-limb amputees upon receiving a new device. It was suggested that, while these adaptations are to be expected, these changes do not occur in a similar manner across individuals. It was observed that participants for this study exhibited differing levels of confidence when using the TAP. It should be noted that the participant who showed the most confidence in the TAP used a torsion shock adapter for their daily prosthesis, and they were also very active. Conversely, the participant who presented less confidence when using the TAP used a rigid pylon for their daily prosthesis, and, based on conversation, they seemed to be not as active. It could be hypothesized that the dynamic nature of the TAP could be more easily adapted to given a familiarity with dynamic prosthetic components.

This study had two main hypotheses for each walking regime: (1) there exists a CR that minimizes peak transverse-plane moment and (2) there exists a CR that maximizes satisfaction. While there does appear to be a distinct torque range for each CR, the torque marginal means and standard errors overlap enough that there is not a distinguishable difference between them. Revisiting the study's small sample size, there are not enough participants to confidently infer conclusions for the entire population of individuals who wear lower-limb prostheses. Figure 4.3 seems to be implying that there exists a difference between the zero CR and at least one of the off-zero CRs for each walking regime. User satisfaction was gauged with the socket comfort

score metric. This metric yielded very similar answers each time it was prompted. Based on participant feedback, the prompt was asking the wrong question given that it focused on the socket fit which is often attributed to a prosthetist's ability to properly fit a custom socket. Assuming that the participant's prosthetist properly fit their prescribed socket, it would make sense that this socket comfort score would not change much if at all given that the TAP's intervention is only apparent during gait. A better question could have asked how the socket felt at the residual limb-socket interface. This question could focus on how the user felt while walking with the device as opposed to the general socket fit. Participants were generally asked for additional feedback for each CR when prompted with the socket comfort score. A CR of 1:2 was often described by one participant as "rattling" and "feels loose" as if this were the most unstable condition. This could be attributed to the fact that this CR has the largest range of motion to rotate through for the same, self-selected walking speed. The CRs 1:4 and 1:3 were both described at one point as "different in the toe" and "lighter in the toe" which was elaborated as the flexing of the foot was different at TO. At TO the TAP is designed to return to a neutral position. Perhaps the 1:4 and 1:3 comments had to do with the peak rotation of the TAP during push-off and how much the TAP needed to rotate to return to neutral.

One of the main outcome metrics of the TAP is socket torque. This is measured indirectly by recording the motor's current draw and then scaling this value by the motor-specific torque constant. Socket torque is then interpreted as proportional to this value. One of the benefits to using this method is a simplification of hardware and design assuming an accurate current measure is achieved. One of the downsides to not using a direct measurement is that there can be a significant amount of space between where the motor's shaft is rotating on the device and the user's socket-limb interface. This space can possibly modify the signal by whatever transfer

function defines that space's material(s) and structure(s). A possible method to remove some undesirable modification of the true signal between the sensor location and the socket would be to use a load cell in series with the socket. Using a load cell in this location will shorten the distance between the sensor and measurand. Pew et al. [26] used this method with the iPecs 6-axis load cell to read transverse plane moments. The drawback to using an in-series load cell is the build height it adds to the device. The TAP is already tall enough that using a full-length pylon to make up length was not required for any of the participants. If any length needed to be added, then any combination of small double female stat adapters, tube clamp adapters, shoe shims, and pylon shims were used. If the goal is to measure the torsional loads at the socket-residual limb interface, then a direct measure in the socket would be an ideal method. Swanson et al. [27] in 2017 developed a socket insert with multiple sensor types to record clinically relevant data. They showed that sensor data could be recorded both in and out of the lab; however, the design and fabrication of the instrumented inserts takes a significant amount of time since this is still a developing area of research.

Chapter 5:
Conclusions and Future Work

This chapter summarizes the work presented in this thesis and provides suggestions for future work in this area. The primary contributions of this thesis are as follows: (1) iteration and development of a powered prosthesis that controls transverse plane ankle rotation for individuals with below-knee amputations, (2) development of a control strategy that takes into account changing body weight during gait, and (3) human subject testing of the TAP.

5.1 Development of the TAP

The TAP is an untethered, battery-powered prosthesis that actively changes rotation in the transverse plane at the ankle based on an approximated sagittal plane ankle angle. The new iteration electrical design concentrated all of the control system electronics to one side of the TAP and the battery to the other opposite side. Using rotary switches to control user settings created an entirely self-contained device that does not need a peripheral device such as a laptop to operate. The only time a computer is needed is to adjust sagittal-transverse plane mapping values specific to the category and size of the prosthetic foot in use and to adjust the amputation side to the current user. The use of strain gauges to approximate sagittal ankle angle in the absence of a physical ankle joint is a novel solution to this problem.

If the TAP were iterated on again, then the electronics could be simplified and improved. The first thing that could be replaced would be the load cell amplifiers used to amplify the strain gauge signals. The current Sparkfun amplifiers are digital and have a sample rate of 80 Hz which is significantly slower than the control loop rate of 1 kHz. These digital amplifiers could be replaced by analog amplifiers, such as an instrumentation amplifier. This change could

significantly reduce the footprint of the TAP's PCB and give a finer strain gauge signal to the controller.

5.2 Development of the Controller

The TAP's controller implements a linear PID scheme with gain scheduling. The gains used were manually tuned under body weight using custom adapter boots that allowed an able-bodied user to walk on the TAP. Gain scheduling allowed for the controller to be adjusted for fluctuating body weight at different phases in the gait cycle. The controller achieves the desired transverse rotation angles corresponding to the current CR setting.

The drawback of using a linear PID to control the motor is that gait is nonlinear. These nonlinearities are due to multiple factors, such as fluctuating GRFs within a single stride, variable walking speeds that can scale GRFs and change gait timings, and muscles that can tire over time and act differently. The current PID controller also does not have any proper modeling of any kind, such as disturbance rejection. Future work could include a more advanced controller for the more up-to-date hardware compared to the first iteration. Revisiting the adaptive controller scheme presented by Olson with the original TAP might be a scheme worth implementing.

5.3 Human Subject Testing

Three male participants with transtibial amputation tested the TAP under CRs ranging from 0 to 1:2 and under three walking regimes: ST, PI, PO. Motor torque and socket comfort score were recorded to find if changing CRs created any statistically significant differences within a walking regime. Motion capture and force plate data were used to calculate joint angles, joint powers, GRFs, and UD powers. These values were analyzed to find if changing CRs did not

create any statistically significant differences in gross joint kinematics and kinetics. rANOVAs showed that there were no significant differences found for any of these cases.

Future work needs to be focused on testing more participants. Currently the study population is too small to have any statistical power, and the results only apply to the study's sample population. Testing a larger, more diverse sample population will improve the generalizability of the results.

References

[1] A. G. Schache and R. Baker, "On the expression of joint moments during gait," *Gait Posture*, vol. 25, no. 3, pp. 440–452, 2007, doi: 10.1016/j.gaitpost.2006.05.018.

[2] C. L. Brockett and G. J. Chapman, "Biomechanics of the ankle," *Orthop. Trauma*, vol. 30, no. 3, pp. 232–238, 2016, doi: 10.1016/j.mporth.2016.04.015.

[3] M. P. Kadaba, H. K. Ramakrishnan, and M. E. Wootten, "Measurement of lower extremity kinematics during level walking," *J. Orthop. Res.*, vol. Vol. 8, no. 3, pp. 383–392, 1990, doi: 10.1007/978-1-4471-5451-8_100.

[4] A. Arndt, P. Westblad, I. Winson, T. Hashimoto, and A. Lundberg, "Ankle and subtalar kinematics measured with intracortical pins during the stance phase of walking," *Foot Ankle Int.*, vol. 25, no. 5, pp. 357–364, 2004, doi: 10.1177/107110070402500514.

[5] C. H. BARNETT and J. R. NAPIER, "The axis of rotation at the ankle joint in man; its influence upon the form of the talus and the mobility of the fibula.," *J. Anat.*, vol. 86, no. 1, pp. 1–9, 1952, [Online]. Available: http://www.ncbi.nlm.nih.gov/pubmed/14907546%0Ahttp://www.pubmedcentral.nih.gov/articlerender.fcgi?artid=PMC1273922.

[6] A. D. Segal, M. S. Orendurff, J. M. Czerniecki, J. Schoen, and G. K. Klute, "Comparison of transtibial amputee and non-amputee biomechanics during a common turning task," *Gait Posture*, vol. 33, no. 1, pp. 41–47, Jan. 2011, doi: 10.1016/j.gaitpost.2010.09.021.

[7] K. C. Flick, M. S. Orendurff, J. S. Berge, A. D. Segal, and G. K. Klute, "Comparison of human turning gait with the mechanical performance of lower limb prosthetic transverse rotation adapters.," *Prosthet. Orthot. Int.*, vol. 29, no. 1, pp. 73–81, Apr. 2005, doi: 10.1080/03093640500088120.

[8] A. D. Segal, M. S. Orendurff, J. M. Czerniecki, J. B. Shofer, and G. K. Klute, "Transtibial amputee joint rotation moments during straight-line walking and a common turning task with and without a torsion adapter," vol. 46, no. 3, pp. 375–384, 2009, doi: 10.1682/JRRD.2008.06.0070.

[9] M. S. Orendurff, J. A. Schoen, B. C. Glaister, G. C. Bernatz, E. A. Huff, A. D. Segal, and G. K. Klute, "Joint rotation torques during a common turning task," *Gait Posture*, vol. 24, no. 2, pp. S201–S203, Dec. 2006, doi: 10.1016/j.gaitpost.2006.11.139.

[10] M. S. Orendurff, A. D. Segal, J. S. Berge, K. C. Flick, D. Spanier, and G. K. Klute, "The kinematics and kinetics of turning: Limb asymmetries associated with walking a circular path," *Gait Posture*, vol. 23, no. 1, pp. 106–111, Jan. 2006, doi: 10.1016/j.gaitpost.2004.12.008.

[11] L. W. Lamoureux and C. W. Radcliffe, "Functional analysis of the UC-BL shank axial rotation device," *Prosthet. Orthot. Int.*, vol. 1, no. 2, pp. 114–118, Aug. 1977, doi: 10.3109/03093647709164619.

[12] A. D. Segal, M. S. Orendurff, J. M. Czerniecki, J. B. Shofer, and G. K. Klute, "Local dynamic stability of amputees wearing a torsion adapter compared to a rigid adapter during straight-line and turning gait," *J. Biomech.*, vol. 43, no. 14, pp. 2798–2803, Oct. 2010, doi: 10.1016/j.jbiomech.2010.05.038.

[13] N. M. Olson and G. K. Klute, "Design of a transtibial prosthesis with active transverse plane control," *J. Med. Devices, Trans. ASME*, vol. 9, no. 4, Dec. 2015, doi: 10.1115/1.4031072.

[14] N. M. Olson, "Transverse-Plane Ankle Rotation for Lower-Limb Amputees Using Two

Novel Prostheses," University of Washington, 2016.
[15] A. Lundberg, O. K. Svensson, and G. Nemeth, "THE AXIS OF ROTATION OF THE ANKLE JOINT," 1989.
[16] P. Lundgren, C. Nester, A. Liu, A. Arndt, R. Jones, A. Stacoff, P. Wolf, and A. Lundberg, "Invasive in vivo measurement of rear-, mid- and forefoot motion during walking," *Gait Posture*, vol. 28, no. 1, pp. 93–100, 2008, doi: 10.1016/j.gaitpost.2007.10.009.
[17] W. S. Erdmann, "Geometry and inertia of the human body - review of research," *Acta of Bioengineering and Biomechanics*, vol. 1, no. 1. pp. 23–35, 1999.
[18] W. Dempster, "Space requirements of the seated operator Geometrical, kinematic, and mechanical aspects of the body." 1955.
[19] D. A. Winter, *Biomechanics and Motor Control of Human Movement: Fourth Edition*. 2009.
[20] C. D. Fryar, M. D. Carroll, Q. Gu, J. Afful, and C. L. Ogdeb, "Anthropometric Reference Data for Children and Adults: United States, 2015–2018," *Natl. Cent. Heal. Stat. Vital Heal. Stat*, vol. 3, no. 46, pp. 1–44, 2021, [Online]. Available: https://www.cdc.gov/nchs/products/index.htm.
[21] A. D. Segal, K. M. Cyr, C. J. Stender, E. C. Whittaker, M. E. Hahn, M. S. Orendurff, W. R. Ledoux, and B. J. Sangeorzan, "A three-year prospective comparative gait study between patients with ankle arthrodesis and arthroplasty," *Clin. Biomech.*, vol. 54, no. August 2017, pp. 42–53, 2018, doi: 10.1016/j.clinbiomech.2018.02.018.
[22] K. Z. Takahashi, T. M. Kepple, and S. J. Stanhope, "A unified deformable (UD) segment model for quantifying total power of anatomical and prosthetic below-knee structures during stance in gait," *J. Biomech.*, vol. 45, no. 15, pp. 2662–2667, 2012, doi: 10.1016/j.jbiomech.2012.08.017.
[23] D. A. Winter and S. E. Sienko, "Biomechanics of below-knee amputee gait," *J. Biomech.*, vol. 21, no. 5, pp. 361–367, 1988, doi: 10.1016/0021-9290(88)90142-X.
[24] J. D. Smith, A. E. Ferris, G. D. Heise, R. N. Hinrichs, and P. E. Martin, "Oscillation and reaction board techniques for estimating inertial properties of a below-knee prosthesis," *J. Vis. Exp.*, no. 87, pp. 1–15, 2014, doi: 10.3791/50977.
[25] J. A. Kent, N. Stergiou, and S. R. Wurdeman, "Dynamic balance changes within three weeks of fitting a new prosthetic foot component," *Gait Posture*, vol. 58, pp. 23–29, Oct. 2017, doi: 10.1016/j.gaitpost.2017.07.003.
[26] C. Pew, A. D. Segal, R. R. Neptune, and G. K. Klute, "Ideal operating conditions for a variable stiffness transverse plane adapter for individuals with lower-limb amputation," *J. Biomech.*, vol. 96, Nov. 2019, doi: 10.1016/j.jbiomech.2019.109330.
[27] E. C. Swanson, J. B. McLean, K. J. Allyn, C. B. Redd, and J. E. Sanders, "Instrumented socket inserts for sensing interaction at the limb-socket interface," *Med. Eng. Phys.*, vol. 51, pp. 111–118, Jan. 2018, doi: 10.1016/j.medengphy.2017.11.006.